

# Cyr61 from adipose-derived stem cells promotes colorectal cancer metastasis and vasculogenic mimicry formation *via* integrin $\alpha_V\beta_5$

Zhenxing Liang<sup>1,2,3</sup>, Huashan Liu<sup>1,2,3</sup>, Yunfeng Zhang<sup>1</sup>, Li Xiong<sup>4</sup>, Ziwei Zeng<sup>1</sup>, Xiaowen He<sup>1</sup>, Fengwei Wang<sup>5</sup>, Xianrui Wu<sup>1,2,3</sup> and Ping Lan<sup>1,2,3</sup> 

1 Department of Colorectal Surgery, The Sixth Affiliated Hospital, Sun Yat-sen University, Guangzhou, China

2 Guangdong Provincial Key Laboratory of Colorectal and Pelvic Floor Diseases, The Sixth Affiliated Hospital, Sun Yat-sen University, Guangzhou, China

3 Bioland Laboratory, Guangzhou Regenerative Medicine and Health Guangdong Laboratory, Guangzhou, China

4 Department of Endocrinology, The First Affiliated Hospital of Sun Yat-sen University, Guangzhou, China

5 State Key Laboratory of Oncology in South China, Sun Yat-sen University Cancer Center, Guangzhou, China

## Keywords

adipose-derived stem cells; colorectal cancer; Cyr61; metastasis and vasculogenic mimicry formation

## Correspondence

F. Wang, State Key Laboratory of Oncology in South China, Sun Yat-Sen University Cancer Center, No. 651, Dongfeng Road East, 510060 Guangzhou, China

Fax: +86-20-87343170

Tel: +86-20-87343193

E-mail: wangfengw@sysucc.org.cn

X. Wu and P. Lan, The Sixth Affiliated Hospital, Sun Yat-sen University, 26 Yuancun Erheng Rd, Guangzhou, Guangdong 510655 China

Fax: +011-86-20-38254166

Tel: +86-020-38255801

E-mails: wuxianr5@mail.sysu.edu.cn (XW);

lanping@mail.sysu.edu.cn (PL)

Zhenxing Liang and Huashan Liu contributed equally to this study.

(Received 14 January 2021, revised 14 April 2021, accepted 14 May 2021, available online 1 June 2021)

doi:10.1002/1878-0261.12998

Adipose-derived stem cells (ADSCs) play a vital role in colorectal cancer (CRC) progression, but the mechanism remains largely unknown. Herein, we found that ADSCs isolated from CRC patients produced more cysteine-rich 61 (Cyr61) than those from healthy donors, and the elevated serum Cyr61 levels were associated with advanced TNM stages. Moreover, serum Cyr61 displayed a better diagnostic value for CRC compared to carcinoembryonic antigen (CEA) and carbohydrate antigen (CA19-9). Mechanistically, integrin  $\alpha_V\beta_5$  was identified as the functional receptor by which Cyr61 promotes CRC cell metastasis *in vitro* and *in vivo* by activating the  $\alpha_V\beta_5$ /FAK/NF- $\kappa$ B signaling pathway. In addition, Cyr61 promotes vasculogenic mimicry (VM) formation, thereby promoting tumor growth and metastasis through a  $\alpha_V\beta_5$ /FAK/HIF-1 $\alpha$ /STAT3/MMP2 signaling cascade. Histologically, xenografts and clinical samples of CRC both exhibited VM, which was correlated with HIF-1 $\alpha$  and MMP2 activation. Notably, we demonstrated the synergistic effect of combined anti-VM therapy (integrin  $\alpha_V\beta_5$  inhibitor) and anti-VEGF therapy (bevacizumab) in patient-derived xenograft models. Further investigation showed that CRC cell-derived exosomal STAT3 promoted Cyr61 transcription in ADSCs. These findings indicate that Cyr61 derived from ADSCs plays a critical role in promoting CRC progression *via* integrin  $\alpha_V\beta_5$  and provides a novel antitumor strategy by targeting Cyr61/ $\alpha_V\beta_5$ .

## Abbreviations

ADSCs, adipose-derived stem cells; AUC, area under the ROC curve; CRC, colorectal cancer; CTCs, circulating tumor cells; Cyr61, cysteine-rich 61; PAS, periodic acid-Schiff; PDX, patient-derived xenograft; ROC, receiver operating characteristic; VM, vasculogenic mimicry.

## 1. Introduction

Colorectal cancer (CRC) is one of the most common carcinomas worldwide, accounting for 8% of cancer incidence and cancer-related deaths in 2018 [1]. Distant metastasis accounts for ~90% of cancer-related deaths due to limited treatment options [2,3]. However, the molecular mechanisms of metastasis remain to be fully elucidated.

Adipose tissue is an endocrine organ, and obesity is a national and international public health concern now [4,5]. Obesity has been reported to be a risk factor for several chronic diseases, including colon cancer [6]. Adipose-derived stem cells (ADSCs) exist widely in adipose tissue and have the ability to differentiate into numerous cells [7]. The impacts of ADSCs on cancer progression are controversial. Although some studies have shown a protective effect of ADSCs mediated by suppressing tumor growth and stimulating apoptosis [8], most studies held the opinion that ADSCs promote tumor progression by influencing the tumor microenvironment [9–12]. ADSCs can differentiate into carcinoma-associated fibroblasts to promote tumor proliferation [13,14]. In addition, ADSCs secrete multiple cytokines and growth factors, such as TGF $\beta$ 1, insulin-like growth factor, and VEGF, which contribute to aggressive tumor behavior [15–17]. Nevertheless, some novel ADSCs secreted cytokines still remain unexploited.

Cysteine-rich 61 (Cyr61), also known as CCN1, belongs to the CCN protein family. Previous studies found that Cyr61 was upregulated in the serum of certain cancers and associated with poor prognosis, such as breast cancer [18], gastric cancer [19], hepatocellular carcinoma [20], and CRC [21]. Cyr61 has diverse biological functions, including promoting cell migration, proliferation, survival, and differentiation, through binding to cell-specific integrin receptors [22]. For example, in endothelial cells and vascular smooth muscle cells, Cyr61 stimulates cell migration *via* binding to  $\alpha_v\beta_3$  and  $\alpha_6\beta_1$  [23]. In gastric adenocarcinoma cells, Cyr61 activates the NF- $\kappa$ B/cyclooxygenase-2 signaling pathway through binding to integrin  $\alpha_v\beta_3$  [24]. In CRC, Cyr61 has been shown to be upregulated and can cooperate with integrin  $\alpha_v\beta_5$  to promote CRC cell migration [25–27]. Estrada *et al.* [28] reported that Cyr61 which is secreted by bone marrow-derived mesenchymal stem cells is able to promote angiogenesis. However, the biological functions, whether integrin  $\alpha_v\beta_5$  was the functional receptor, and source of Cyr61 in CRC remain not fully clarified.

In this study, we found that CRC-associated ADSCs (ADSCs-CRC) secreted more Cyr61 than the

controls (ADSCs-NC). Elevated serum Cyr61 levels were associated with advanced TNM stages. Mechanistically, we identified that integrin  $\alpha_v\beta_5$  was the functional receptor of Cyr61 and Cyr61 promotes CRC metastasis and vasculogenic mimicry (VM) formation by activating the signaling pathway downstream of integrin  $\alpha_v\beta_5$ . Moreover, synergistic effect of anti-VM by integrin  $\alpha_v\beta_5$  inhibitor and anti-VEGF by bevacizumab therapy was found in patient-derived xenograft (PDX) models. Collectively, our findings indicate that Cyr61 derived from ADSCs plays a critical role in promoting CRC progression *via* integrin  $\alpha_v\beta_5$  and provides a novel antitumor strategy based on targeting the Cyr61/ $\alpha_v\beta_5$ .

## 2. Material and methods

### 2.1. ADSC isolation and characterization

After obtaining informed consent, adipose tissues were obtained from omentum majus from CRC patients and control donors undergoing surgery for non-neoplastic disease and were split as previously studies [29]. First, adipose tissues were washed with PBS to remove debris and red blood cells. Adipose tissues were cut into pieces and treated with 0.25% collagenase type I for 30 min at 37 °C. Then, equal volume Dulbecco's modified Eagle medium (DMEM; Gibco, Thermo Fisher Scientific, St Peters, MO, USA) with 10% FBS (Gibco) was added to neutralize the collagenase activity. Finally, cells were plated on dishes in DMEM with 1 g·L<sup>-1</sup> glucose and 10% FBS. After the third passage, we identified the cells by flow cytometric analysis with three stem cell positive markers, CD105, CD90, and CD73, and seven negative markers CD45, CD79a, CD19, CD34, CD14, CD11b, and HLA-DR.

### 2.2. Patients and samples

Cyr61 levels were analyzed in serum samples from healthy donors ( $n = 90$ ) and CRC patients ( $n = 364$ ). Integrin  $\beta_5$  levels were analyzed in 10 paired CRC tissue samples. 293 samples of CRC formalin-fixed, paraffin-embedded tissues were used for integrin  $\beta_5$  expression detection and Kaplan–Meier survival analysis. None of the patients received chemotherapy or radiotherapy before surgery. All the samples were collected from the Sixth Affiliated Hospital of Sun Yat-sen University. All samples were stored at  $-80$  °C refrigerator until further use.

### 2.3. Cell culture and cell treatment

The CRC cell lines HCT8, HCT116, DLD1, and human embryonic kidney 293T cells were purchased from the American Type Culture Collection (ATCC, Washington, DC, USA). All cells were cultured in DMEM (Gibco) supplemented with 10% FBS (Gibco) at 37 °C under 5% CO<sub>2</sub>. Recombinant human Cyr61 (rCyr61) protein was purchased from Amyjet Scientific. The neutralizing anti-Cyr61 antibody and the integrin  $\beta_5$  inhibitor (EMD121974; EMD) were purchased from Thermo Fisher Scientific and Selleck (Houston, TX, USA), respectively. Different concentrations of rCyr61, neutralizing antibody, and inhibitor were added prior to experiments.

### 2.4. ELISA

Cyr61 ELISA kit (RayBiotech, Atlanta, GA, USA) was used to detect the Cyr61 level in supernatants of ADSCs and serum samples according to the manufacturer's protocol. ELISACALC software (ELISA Calc, Shanghai, China) was used to generate standard curve.

### 2.5. RNA extraction and real-time PCR

Total RNA was isolated from cells by TRIzol Reagent (Thermo Fisher Scientific). ReverTra Ace qPCR RT Kit (Toyobo, Kita-ku, Osaka, Japan) was used to perform reverse transcription according to the manufacturer's instructions. The Applied Biosystems 7500 Sequence Detection system was used to carry out quantitative real-time reverse transcription PCR (qRT-PCR) with the SYBR Green PCR Master Mix (Applied Biosystems, Foster City, CA, USA). We generated standard curves and applied the  $2^{-\Delta\Delta CT}$  method with normalized to 18S rRNA. All the gene-specific primers were obtained from Invitrogen (Thermo Fisher Scientific), and the oligonucleotide sequences are listed in Table S4.

### 2.6. Western blot analysis

Cell and tissue samples were lysed with radio-immunoprecipitation assay buffer (RIPA) with protease and phosphatase inhibitor cocktail (Promega, Fitchburg, WI, USA). Proteins were separated by SDS/PAGE and then transferred to polyvinylidene fluoride (PVDF) membranes by the Trans-Blot System (Bio-Rad, Hercules, CA, USA). The membranes were blocked by milk and then incubated with specific primary antibodies against Cyr61 (Abcam, Cambridge, MA, USA, 1 : 1000), integrin  $\beta_5$  (Cell Signaling

Technology, Danvers, MA, USA, CST, 1 : 1000), FAK (CST, 1 : 1000), p-FAK (CST, 1 : 1000), P65 (CST, 1 : 1000), GAPDH (Abcam, 1 : 1000), MEK (CST, 1 : 1000), p-MEK (CST, 1 : 1000), ERK (CST, 1 : 1000), p-ERK (CST, 1 : 1000), STAT3 (CST, 1 : 1000), p-STAT3 (CST, 1 : 1000), MMP2 (Abcam, 1 : 2000), and HIF-1 $\alpha$  (Abcam, 1 : 500). Finally, membranes were incubated with a specific secondary antibody and visualized by ECL Blotting Detection Reagents. GAPDH served as a control for western blot analysis.

### 2.7. Cell linages isolation in CRC tissues

Fresh tissue was chopped with a sterile scalpel and then digested for 1 h at 37 °C using collagenase digestion medium (RPMI-medium, collagenase type IV 1 mg·mL<sup>-1</sup> and DNase I 150 U·mL<sup>-1</sup>) to obtain single cell suspension. Lymphocytes, macrophages, endothelial cells, and CRC cells were purified with CD3<sup>+</sup> microbeads (Miltenyi Biotec, Bergisch Gladbach, Germany, 130-050-101), CD14<sup>+</sup> microbeads (Miltenyi Biotec, 130-050-201), CD31<sup>+</sup> microbeads (Miltenyi Biotec, 130-091-935), and EpCAM<sup>+</sup> microbeads (Miltenyi Biotec, 130-061-101), respectively. Finally, cells were plated in adherent conditions in growth medium (DMEM, Pen-Strep 1X, 10% FBS) and passaged regularly to obtain fibroblasts.

### 2.8. Cell migration assay

Cell migration assays were performed with 24-well plates with 8  $\mu$ m pore size chamber inserts (Corning, New York, NY, USA). In general,  $5 \times 10^4$  cells resuspended with 200  $\mu$ L serum-free DMEM were seeded in the upper chamber well and 800  $\mu$ L of DMEM with 10% FBS was added into the lower chamber. After 24 h, cells migrating through the membrane were fixed with 4% paraformaldehyde for 15 min and then stained with 0.1% crystal violet for 15 min. The cells were viewed under an inverted microscope (DMI4000B; Leica, Wetzlar, Germany) and quantified using software IMAGEJ (Bethesda Softworks LLC, Rockville, MD, USA).

### 2.9. Wound-healing assay

A total of  $2 \times 10^6$  cells were seeded in six-well plates and incubated until confluency was reached. A 100  $\mu$ L pipette tip was used to create a rectilinear scratch. After 24 h, cells were fixed with 4% paraformaldehyde for 15 min and then stained with 0.1% crystal violet for 15 min. An inverted microscope (DMI4000B; Leica) was utilized to image the wound closure.

## 2.10. Cell counting

A total of  $5 \times 10^4$  cells were resuspended in DMEM with 10% FBS and seeded in a 12-well plate. The cells were released by trypsinization 3 days later, and cell numbers were counted immediately.

## 2.11. Vector construction and generation of stable cell lines

The methods for vector construction and generation of stable cell lines were described in our previous study [30]. The oligonucleotides to suppress integrin  $\beta_5$  expression were designed by RiboBio (Guangzhou, China). After we verified their knockdown efficiency, they were cloned into lentiviral expression vector pLKO.1-Pur (Addgene, Cambridge, MA, USA). The plasmids were verified by sequencing. Empty vector pLKO.1-Pur carrying a scrambled shRNA served as a control. 293T cells were incubated with the constructed vectors, pMD2G and psPAX2 (Addgene), according to the manufacturer's protocol. 0.22  $\mu\text{m}$  PVDF filters were used to filter 293T cells supernatant, and then, the supernatant was added into the plate to infect DLD1, HCT116, and HCT8 cells. The oligonucleotide sequences for vector construction are listed in Table S4.

## 2.12. Mass spectrometry assay

The gel was chopped into small fragments with a razor blade, destained, and subjected to digestion by modified porcine trypsin (50–100 ng per digestion; Promega). After trypsin digestion, peptides were dissolved in 0.1% FA and 2% ACN, directly loaded onto a reversed-phase analytical column (75  $\mu\text{m}$  i.d.  $\times$  150 mm, packed with Acclaim PepMap RSLC C18, 2  $\mu\text{m}$ , 100  $\text{\AA}$ , nanoViper, Thermo Fisher Scientific). The gradient was comprised of an increase from 5% to 50% solvent B (0.1% FA in 80% ACN) over 40 min, climbing to 90% in 5 min, and then holding at 90% for the 5 min. All at a constant flow rate of 300  $\text{nL}\cdot\text{min}^{-1}$ . The MS analysis was performed on Q Exactive hybrid quadrupole-Orbitrap mass spectrometer (Thermo Fisher Scientific). The peptides were subjected to NSI source followed by tandem mass spectrometry (MS/MS) in Q Exactive<sup>TM</sup> (Thermo Fisher Scientific) coupled online to the UPLC. Intact peptides were detected in the Orbitrap at a resolution of 70 000. Peptides were selected for MS/MS using NCE setting as 27; ion fragments were detected in the Orbitrap at a resolution of 17 500. A data-dependent procedure that alternated between one MS scan

followed by 20 MS/MS scans was applied for the top 20 precursor ions above a threshold ion count of 1E4 in the MS survey scan with 30.0s dynamic exclusion. The electrospray voltage applied was 2.0 kV. Automatic gain control (AGC) was used to prevent overfilling of the ion trap; 1E5 ions were accumulated for generation of MS/MS spectra. For MS scans, the  $m/z$  scan range was 350–1800  $m/z$ . Fixed first mass was set as 100  $m/z$ . Protein identification was performed with MASCOT software by searching Uniprot\_Aedis Aegypti.

## 2.13. Membrane protein extraction and receptor identification

Cell membrane proteins were extracted using the ProteoExtract Native Membrane Protein Extraction Kit (M-PEK Kit; Calbiochem, Thermo Fisher Scientific) according to manufacturer's recommendation. Before this experiment, cells were treated with 40  $\text{ng}\cdot\text{mL}^{-1}$  rCyr61 for 1 h. The IgG group and 0.1% SDS group served as controls. The SDS-Out Precipitation Kit (Pierce, Thermo Fisher Scientific) was used to remove the SDS. Then, the extracts were incubated with 50  $\mu\text{l}$  beads coupled with IgG or anti-human monoclonal Cyr61 antibody at 37 °C overnight. Finally, proteins were separated by SDS/PAGE and visualized by Coomassie blue staining. The protein-specific bands were excised for mass spectrometric analysis.

## 2.14. Immunohistochemistry and IHC scoring

Paraffin-embedded tissues were deparaffinized with dimethylbenzene followed by antigen retrieval. The tissues were blocked with normal goat serum at 37 °C for 30 min. Next, the tissues were incubated overnight at 4 °C with specific primary antibodies against integrin  $\beta_5$  (Bioss, Boston, MA, USA, 1 : 200), p-FAK (CST, 1 : 600), p-ERK (CST, 1 : 250), p-STAT3 (CST, 1 : 200), MMP2 (Abcam, 1 : 200), HIF-1 $\alpha$  (Abcam, 1 : 100), and CD31 (CST, 1 : 200). Finally, the tissues were incubated with appropriate secondary antibodies and then incubated with 3, 3'-diaminobenzidine (DAB). We evaluated the marker staining results according to a previous study [31]. The staining intensity was graded 4 stages: 0 (none), 1 (weak), 2 (moderate), and 3 (strong). The percentage of expression was graded 5 stages: 0 (< 5% staining), 1 (5–25% staining), 2 (25–50% staining), 3 (50–75% staining), and 4 (> 75% staining). The sum of both scores served as the final score. Two pathologists performed the scoring analyses according to the above criteria.

### 2.15. Immunofluorescence assays

The cells were incubated overnight at 4 °C with specific primary antibodies Cyr61 (Abcam, 1 : 500), integrin  $\beta$ 5 (CST, 1 : 1600), p-FAK (CST, 1 : 100), P65 (CST, 1 : 400), p-MEK (CST, 1 : 500), ERK (CST, 1 : 800), STAT3 (CST, 1 : 100), MMP2 (Abcam, 1 : 250), and HIF-1 $\alpha$  (Abcam, 1 : 1000). Then, cells were incubated with Alexa 488- or Alexa 594-conjugated goat antibodies (Thermo Fisher Scientific) against mouse or rabbit IgG. Finally, the samples were counterstained with DAPI and imaged with confocal laser-scanning microscope (Leica TCS-SP8).

### 2.16. *In vitro* vasculogenic mimicry assay

Briefly, 30  $\mu$ L of Matrigel (BD, BD Biosciences, Franklin Lakes, NJ, USA) was plated in 96-well plates and incubated at 37 °C for 30 min to allow polymerization. Next,  $1 \times 10^5$  cells per well were added to the Matrigel layer and grown for 12 h. Randomized fields were captured using an inverted microscope, and tubes were quantified from each image.

### 2.17. Flow cytometric analysis

Adipose-derived stem cells were incubated with fluorochrome-conjugated specific antibodies and matched control IgG at room temperature for 30 min. Then, flow cytometry (BD Biosciences) was used to analyze the cells. The data were analyzed by software FLOWJO software (v10.0.7, Tree Star, San Carlos, CA, USA).

### 2.18. Luciferase assays

Cyr61 promoter sequences (from -2000 to +100 relative to the transcription start site) and sequential deletion were cloned into pGL3-Basic vector. STAT3 cDNA was cloned in pcDNA3.1. These plasmids were transfected into ADSCs by Lipofectamine 3000 (Invitrogen) according to the manufacturer's instructions. A Dual-luciferase Reporter Assay System (Promega) was used according to the manufacturer's instructions.

### 2.19. Exosome extraction and identification

Exosomes were extracted and identified according to our previous study [30]. In briefly, supernatants were harvested and centrifuged sequentially at 300 *g* for 15 min, 2000 *g* for 15 min, 10 000 *g* for 30 min, and 120 000 *g* for 70 min (Beckman Coulter, Brea, CA, USA) twice. Then, Particle Metrix (PMX), transmission

electron microscopy (TEM), and western blot analysis were used to identify the exosomes.

### 2.20. Animal experiments

All animal experiments were approved by the Institutional Animal Care and Use Committee of Sun Yat-sen University, Guangzhou, China. Four- to five-week-old male BALB/c nude mice were purchased from the Animal Experiment Center of Sun Yat-Sen University and were fed in SPF environment. A spleen injection model was used for liver colonization assays ( $n = 5$  per group). We analyzed liver metastasis by autopsy and hematoxylin and eosin staining (H&E). After CRC cells were treated with Cyr61 (20 ng·mL<sup>-1</sup>) for one week,  $1 \times 10^6$  cells in 100  $\mu$ L PBS were intrasplenically injected. An immediate splenectomy was performed following intrasplenic injection. Subcutaneous tumor growth assays were performed as previous study [32] ( $n = 5$  per group). Subcutaneous tumors were evaluated by H&E and immunohistochemistry (IHC). GFP-positive circulating tumor cells (CTCs) in PBMCs of mice were analyzed by flow cytometry as the previous study [33].

### 2.21. Patient-derived xenograft models and intratumoral injection assay

Fresh tumor tissues were obtained from two CRC patients and implanted into NCG mice. When the tumor size reached 1.5 cm<sup>3</sup>, the tumors were divided into equal volume  $\sim 2$  mm<sup>3</sup> and were subcutaneously implanted into 4- to 5-week-old male BALB/c nude mice. When the tumor size reached about 100 mm<sup>3</sup>, all mice were randomized into four groups ( $n = 4$  per group): control group, cilengitide (EMD121974, 10 mg·kg<sup>-1</sup>, once a week) group, bevacizumab (5 mg·kg<sup>-1</sup>, once a week), and EMD121974 plus bevacizumab group. Intratumor injection of rCyr61 (0.2  $\mu$ g·kg<sup>-1</sup>) was performed 24h later after inhibitor intratumor injection. All reagents were injected precisely into the center of the tumors. All mice were sacrificed 4 weeks later, and subcutaneous tumors were subjected to H&E and IHC.

### 2.22. Statistical analysis

GRAPHPAD PRISM Software (GraphPad Software, La Jolla, CA, USA) was used to perform statistical analysis. Two-tailed Student's test, one-way ANOVA, and Pearson's correlation analysis were performed for statistical comparisons. All statistics analysis data are expressed as mean  $\pm$  standard error of the mean. A *P* value < 0.05 was considered statistically significant.

### 2.23. Study approval

All samples from human tissues were collected with written informed consent from donors, and all procedures were performed with the approval of the Institutional Review Board of The Sixth Affiliated Hospital of Sun Yat-sen University. Animal experiments were approved by the Institutional Animal Care and Use Committee of Sun Yat-sen University and conformed to the Guide for the Care and Use of Laboratory Animals of the National Institutes of Health (National Academies Press, 2011) in China.

## 3. Results

### 3.1. Cyr61 expression is upregulated in ADSCs derived from CRC patients

We first identified the characteristics of the ADSCs after isolation. ADSCs exhibited a typical spindle-shaped fibroblast-like appearance (Fig. S1A). Furthermore, ADSCs possessed the capacity for multilineage differentiation into adipocytes (Fig. S1B) and osteocytes (Fig. S1C). Flow cytometric analysis of the cell surface markers showed that the isolated ADSCs were positive for CD105, CD90, and CD73 and were negative for CD45, CD79a, CD19, CD34, CD14, CD11b, and HLA-DR (Fig. S1D). Thus, these data confirmed that ADSCs were successfully isolated.

The CCN protein family comprises six members, including Cyr61 (CCN1), connective tissue growth factor (CTGF, CCN2), nephroblastoma overexpressed protein (Nov, CCN3), wnt-1-induced secreted protein 1 (WISP-1, CCN4), WISP-2 (CCN5), and WISP-3 (CCN6) [34]. These proteins are involved in multiple biological processes, such as cell proliferation, migration, survival, and angiogenesis [35,36], but the functions of these proteins in ADSCs and CRC remain to be fully clarified. We performed qRT-PCR to analyze the mRNA levels of CCN protein family members in ADSCs isolated from nine healthy donors and 11 CRC patients. Among all the CCN protein family members tested, only Cyr61 was upregulated in ADSC-CRC (Fig. S1E, Fig. 1A). Furthermore, ELISAs indicated that ADSCs-CRC secreted abundant amounts of Cyr61 protein into their culture supernatants (Fig. 1B).

Next, ELISAs were performed to analyze Cyr61 protein levels in serum from 90 healthy donors and 364 CRC patients. Serum Cyr61 protein was upregulated in CRC patients and was positively correlated with tumor TNM stages (Fig. 1C,D). By assessing the

relationship between serum Cyr61 and the clinicopathologic characteristics of CRC patients, we found that Cyr61 was significantly elevated in patients with more advanced TNM stages ( $P < 0.001$ ; Table S1). We then conducted receiver operating characteristic (ROC) curve analysis to compare the diagnostic power of Cyr61 with the traditional biomarkers of CRC. The results showed that the area under the ROC curve (AUC) for Cyr61 was 0.933, better than the traditional diagnostic biomarkers (Fig. 1E and Table S2). Furthermore, decision curve analysis showed that Cyr61 levels provided greater net diagnostic power than three traditional biomarkers, regardless of the threshold used (Fig. 1F). Compared with the Cyr61 levels in ADSC culture supernatants, Cyr61 protein secreted by CRC cell lines was negligible (Fig. S1F). Moreover, western blot analysis of tumor tissues and major tumor infiltration cells, such as lymphocytes, macrophages, endothelial cells, and fibroblasts, also showed negligible expression of Cyr61 protein tissues in CRC tissues (Fig. S1G). These data demonstrated that ADSCs-CRC appeared to be the main source of Cyr61 protein and serum Cyr61 may be a potential diagnostic biomarker of CRC.

### 3.2. ADSC-derived Cyr61 promotes CRC cell invasion and migration *in vitro*

To determine whether ADSCs contribute to cancer cell invasion and migration, we employed cell migration and wound-healing assays. For cell migration assays, CRC cells were seeded in the upper wells with ADSCs in the lower wells. For wound-healing assays, ADSCs were seeded in the upper wells with CRC cells in the lower wells. Compared with the ADSCs-NC, ADSCs-CRC significantly promoted cell invasion and migration (Fig. S2A,B). A polyclonal anti-Cyr61 antibody with neutralized function was used to determine the ability of Cyr61 to contribute to cancer cell invasion and migration. Compared with  $10 \mu\text{g}\cdot\text{mL}^{-1}$  IgG, the addition of  $5 \mu\text{g}\cdot\text{mL}^{-1}$  anti-Cyr61 antibody to HCT8 and DLD1 cells reduced the number of invasive cancer cells by 36% and 27%, respectively, and the addition of  $10 \mu\text{g}\cdot\text{mL}^{-1}$  anti-Cyr61 antibody reduced the cell number by 69% and 54%, respectively (Fig. 2A). CRC cells migrated slowly to close the scratched wounds while adding neutralized anti-Cyr61 antibody (Fig. 2B). Furthermore, treatment of HCT8, DLD1, and HCT116 cells with recombinant Cyr61 (rCyr61,  $0\text{--}40 \text{ ng}\cdot\text{mL}^{-1}$ ) enhanced the invasion and migration of cells in a dose-dependent manner (Fig. 2C,D). Cell counting and MTS assays revealed that incubation of CRC cells with ADSCs-CRC significantly promoted

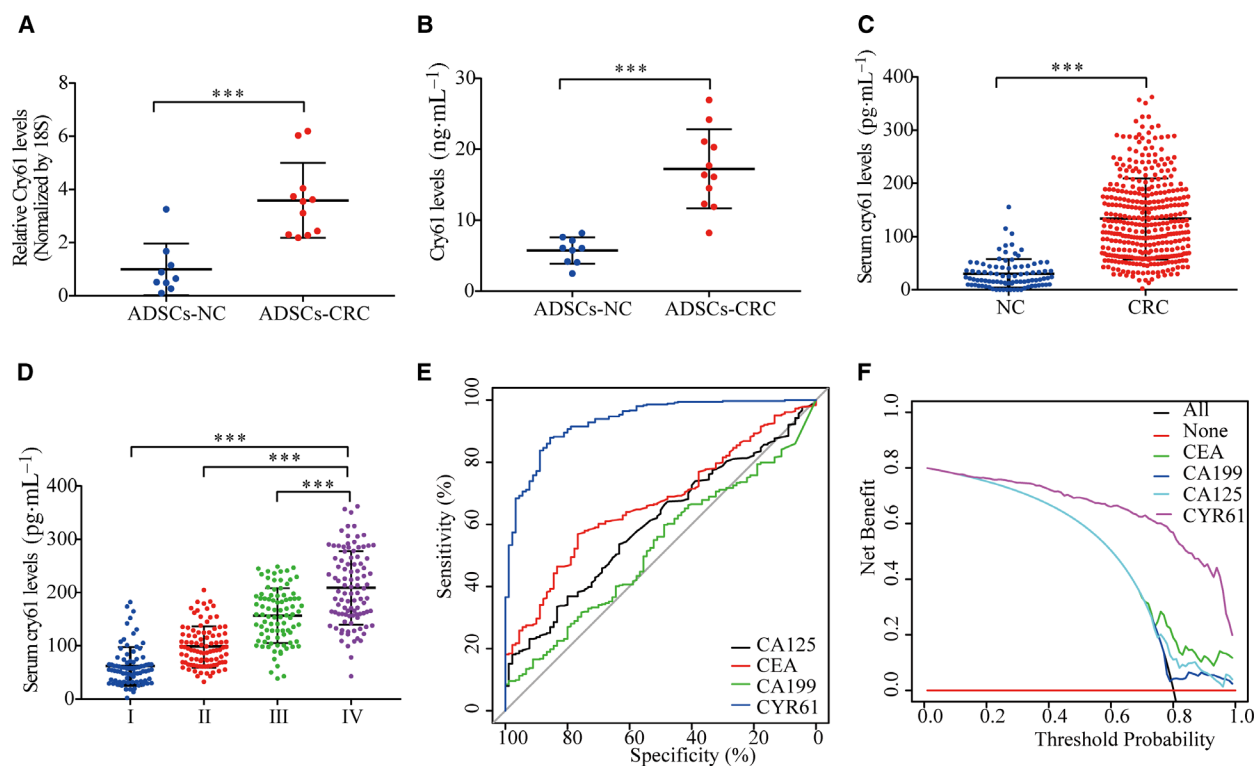


**Fig. 1.** Serum Cyr61 is a diagnostic marker for CRC. (A) qRT-PCR analysis of Cyr61 mRNA levels in ADSCs-NC ( $n = 9$ ) and ADSCs-CRC ( $n = 11$ ). (B) ELISA of Cyr61 levels in the medium of ADSCs-NC ( $n = 9$ ) and ADSCs-CRC ( $n = 11$ ). (C) ELISA of serum Cyr61 levels in healthy donors ( $n = 90$ ) and CRC patients ( $n = 364$ ). (D) ELISA of serum Cyr61 levels in different CRC tumor stages. (E) ROC curves for diagnosis of CRC *via* serum Cyr61, CA125, CEA, or CA199 levels. (F) Decision curve for diagnosis of CRC *via* serum Cyr61, CA125, CEA, or CA199 levels. Values are represented as mean  $\pm$  SD. \*\*\* $P < 0.001$ , by two-tailed Student's *t*-test (A–C) and one-way ANOVA (D).

cell proliferation compared to ADSCs-CRC (Fig. S2C, D). However, adding neutralized antibody to the coculture system did not influence CRC cell proliferation (Fig. S2E,F). Collectively, these data suggested that ADSCs-CRC promoted CRC cell invasion and migration *via* Cyr61.

### 3.3. Integrin $\alpha_V\beta_5$ is the functional receptor of Cyr61

To investigate the existence of a receptor of Cyr61 on the CRC cell membrane, HCT8 cells were treated with rCyr61. Immunofluorescence (IF) assays showed that rCyr61 was localized to the cell membrane, implying the presence of a Cyr61-specific receptor on CRC cell membrane (Fig. 3A). To identify the unknown receptor, we extracted the membranous proteins from HCT8 cells treated with rCyr61. Specific protein bands were detected after immunoprecipitation with Cyr61-specific antibody (Fig. 3B) and were subjected to mass spectrometry. Nine candidate membranous proteins were identified (Table S3). Among these proteins, integrin  $\alpha_V\beta_5$  got the highest score in the mass spectrometry

results and only integrin  $\alpha_V\beta_5$  belonged to the integrin family (Fig. S3A,B). Subsequent western blot analysis with specific antibodies for the detection of integrin  $\alpha_V$  and integrin  $\beta_5$  confirmed the combination of Cyr61 with integrin  $\alpha_V\beta_5$  in HCT8 and DLD1 cells (Fig. 3C). Besides, purified integrin  $\alpha_V\beta_5$  was used to confirm the direct interaction with Cyr61 (Fig. 3D). Furthermore, CRC cells were incubated with rCyr61 and the IF assays results demonstrated that Cyr61 colocalized with integrin  $\alpha_V\beta_5$  on the plasma membrane (Fig. S3D). Following short hairpin RNA (shRNA)-mediated knock-down of integrin  $\beta_5$  expression, Cyr61 localization on the cell surface was decreased (Fig. S3C,D). Moreover, integrin  $\beta_5$  was overexpressed in the majority of CRC cell lines (HCT8, DLD1, and HT29) compared to the normal colonic cell lines HIEC-6 and NCM460 (Fig. 3E).

Next, integrin  $\beta_5$  protein levels were analyzed in 10 CRC patient tissues and matched normal tissues. Western blot analysis indicated that integrin  $\beta_5$  was notably increased in 9 out of 10 CRC tissues (Fig. 3F). To investigate the clinical significance of integrin  $\beta_5$ , we detected integrin  $\beta_5$  expression levels in a large cohort

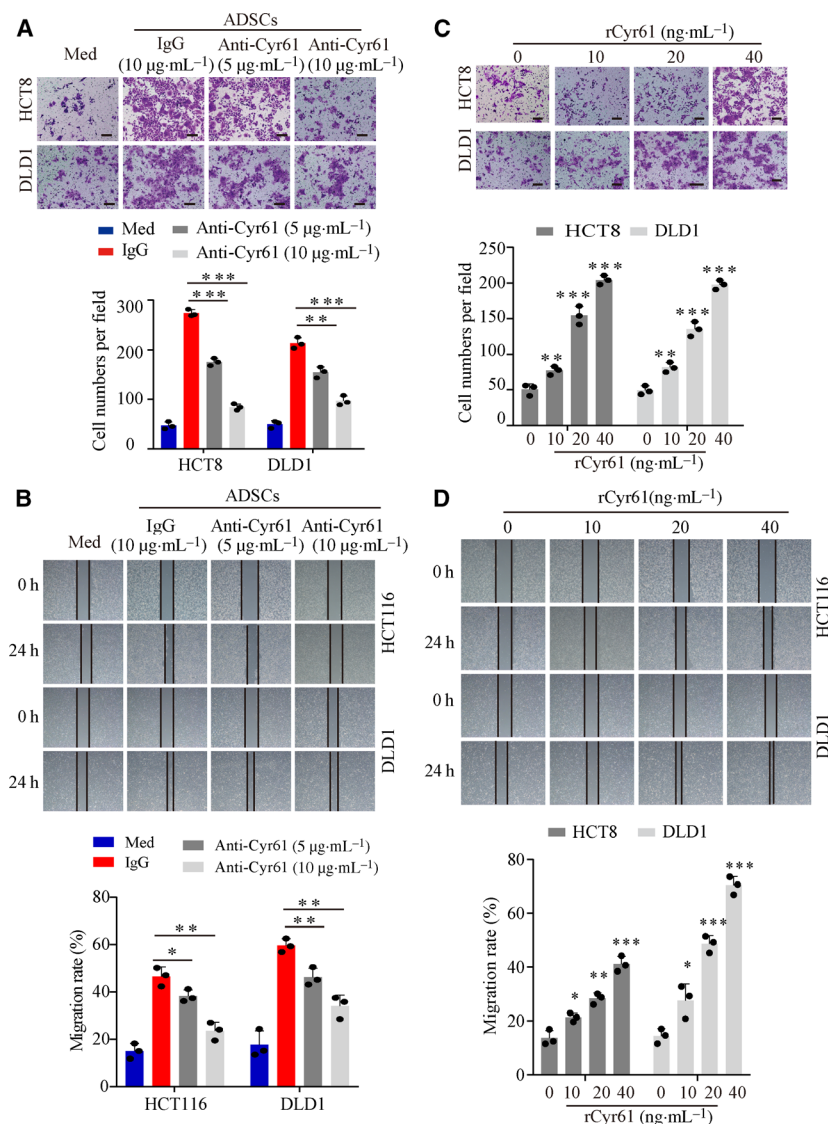


**Fig. 2.** ADSC-derived Cyr61 promotes CRC cell invasion and migration *in vitro*. (A) Representative images of transwell migration assays for HCT8 and DLD1 cells cocultured with culture medium alone (Med) or ADSCs in the presence or absence of 5 or 10 µg·mL<sup>-1</sup> anti-Cyr61 antibody, or isotype-matched IgG control (IgG). Scale bar = 100 µm, *n* = 3. (B) Representative images of wound-healing assays for HCT116 and DLD1 cells cocultured with Med or ADSCs in the presence or absence of an anti-Cyr61 antibody at 5 or 10 µg·mL<sup>-1</sup>, or an IgG. *n* = 3. (C) Representative images of transwell migration assays for HCT8 and DLD1 cells with rCyr61 at different concentration. Scale bar = 100 µm, *n* = 3. (D) Representative images of wound-healing assays for HCT116 and DLD1 cells with rCyr61 at different concentration. *n* = 3. Values are represented as mean ± SD. \**P* < 0.05, \*\**P* < 0.01, \*\*\**P* < 0.001, by one-way ANOVA.

of CRC patients. Immunohistochemical (IHC) analysis also suggested that integrin  $\beta_5$  was upregulated in CRC tissues (Fig. 3G). Moreover, survival analysis showed that high integrin  $\beta_5$  expression was associated with poor overall survival (OS; *P* = 0.002, Fig. 3H) and disease-free survival (DFS) in CRC patients (*P* < 0.001; Fig. 3I). Taken together, integrin  $\alpha_V\beta_5$  was the functional receptor of Cyr61 and played an important role in CRC progression.

### 3.4. Cyr61 promotes CRC cell migration and invasion *via* $\alpha_V\beta_5$ /FAK/NF- $\kappa$ B signaling pathway

To confirm the ability of Cyr61 to promote CRC migration and invasion *via* integrin  $\alpha_V\beta_5$ , we employed the integrin  $\alpha_V\beta_5$  inhibitor EMD 121974

(EMD) and integrin  $\beta_5$ -specific shRNA (sh $\beta_5$ ). Compared with the control group, the number of invasive cancer cells was reduced and CRC cells migrated slowly to close the scratched wounds in the presence of EMD or shRNA (Fig. 4A,B). Aberrant nuclear factor- $\kappa$ B (NF- $\kappa$ B) activation promotes cancer invasion and metastasis in many cancers, including CRC [37,38]. As FAK activates a number of downstream molecules, including NF- $\kappa$ B [39], we hypothesized that Cyr61 binds to integrin  $\alpha_V\beta_5$  to activate the FAK-NF- $\kappa$ B signaling pathway to promote CRC cell migration and invasion. As expected, western blot analysis showed that the protein expression of p-FAK and p-P65 increased following incubation of HCT8 and DLD1 cells with rCyr61 as determined (Fig. 4C and Fig. S4A). Treatment with sh $\beta_5$  or

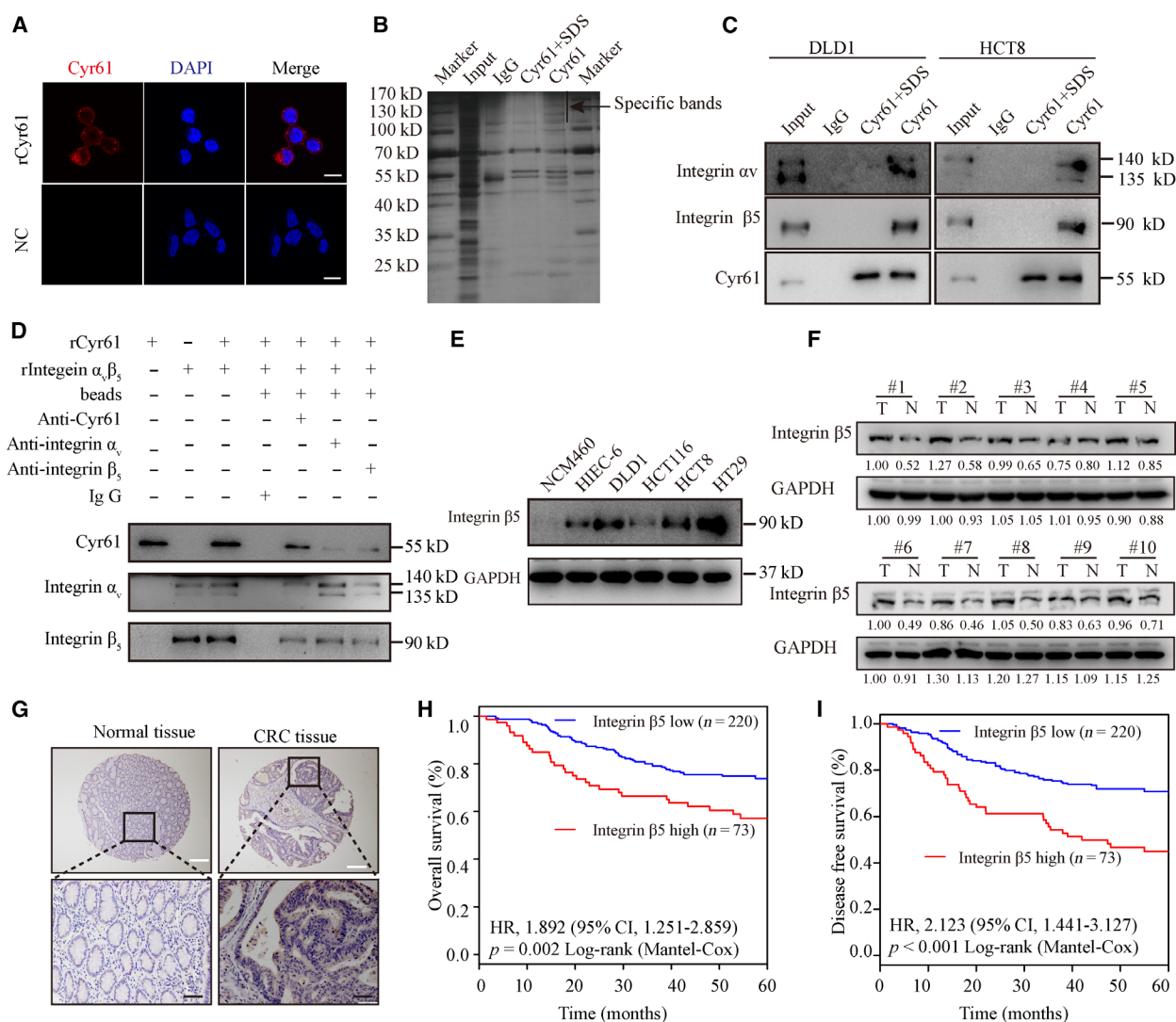


**Fig. 3.** Cyr61 binds to integrin  $\alpha_v\beta_5$  on CRC cells. (A) Confocal microscopy for HCT8 cells in the presence or absence of rCyr61 at 40 ng·mL<sup>-1</sup>. Scale bar = 10  $\mu$ m. (B) Immunoprecipitation of the membrane extracts of rCyr61-treated HCT8 cells with anti-Cyr61 antibody. (C) Western blot validation of mass spectrometric results with anti-integrin  $\alpha_v$ , anti-integrin  $\beta_5$ , and anti-Cyr61 antibody in immunoprecipitation products of the membrane extracts from rCyr61-treated HCT8 and DLD1 cells with anti-Cyr61 antibody. (D) Western blot analysis validation of the direct interaction between Cyr61 and integrin  $\alpha_v\beta_5$ . (E) Western blot analysis of integrin  $\beta_5$  expression in normal colonic cell lines and CRC cell lines. (F) Western blot analysis of integrin  $\beta_5$  expression in 10 CRC tissues and paired normal adjacent tissues. (G) IHC analysis of integrin  $\beta_5$  expression in the paraffin-embedded CRC tissues and paired normal adjacent tissues. White scale bar = 200  $\mu$ m. Black scale bar = 50  $\mu$ m. (H, I) Kaplan–Meier analysis for OS and DFS of CRC patients with low or high expression of integrin  $\beta_5$ .

EMD abrogated the Cyr61-induced  $\alpha_v\beta_5$ /FAK/NF- $\kappa$ B signaling (Fig. 4C and Fig. S4A). Further analysis of the protein levels of p-FAK and subcellular localization of P65 by IF revealed upregulated p-FAK expression and intense nuclear staining of P65 following Cyr61 stimulation. Thus, our results indicated that  $\alpha_v\beta_5$ /FAK/NF- $\kappa$ B signaling pathway is inhibited by sh $\beta_5$  or EMD (Fig. 4D and Fig. S4B).

Next, we performed *in vivo* metastasis assays by intrasplenic injection of nude mice with HCT8 cells pretreated with rCyr61, sh $\beta_5$ , or EMD ( $n = 5$  per group). Incubation of HCT8 with rCyr61 increased the number of metastatic nodules in the liver and decreased the survival time compared to the control group. However, shRNA-mediated knockdown of integrin  $\beta_5$ - or EMD-induced inhibition of the receptor

decreased the number of metastatic nodules and increased the survival time compared to the Cyr61 group (Fig. 4E–H). These findings suggested that Cyr61 promotes CRC cell migration and invasion *via* the integrin  $\alpha_V\beta_5$ /FAK/NF- $\kappa$ B signaling pathway *in vitro* and *in vivo*.

### 3.5. Cyr61 promotes VM formation to promote CRC growth and metastasis

Our previous study indicated that Cyr61 did not influence CRC cell proliferation *in vitro* (Fig. S2E,F). We performed subcutaneous xenograft assays to further confirm this effect *in vivo* ( $n = 5$  per group). Intriguingly, the results suggested that Cyr61 increased the volume and weight of tumors. Treatment with sh $\beta_5$  or EMD abrogated the effect of Cyr61 on tumor growth (Fig. 5A–C). A previous study indicated that Epstein–Barr virus-infected cancer cells promoted VM formation by upregulating the expression of some genes, including Cyr61 [40]. Therefore, we hypothesized that Cyr61 promotes CRC growth by promoting VM formation. The criteria of VM formation were positive for periodic acid-Schiff (PAS) but negative for CD31 (PAS<sup>+</sup>/CD31<sup>−</sup>) and the existence of erythrocytes in the vascular-like channels [41]. The results showed that tumors derived from cells treated with rCyr61 exhibited more VM structures. As expected, treatment with sh $\beta_5$  or EMD decreased the number of VM structures (Fig. 5D,E).

The molecular mechanism of VM formation was complicated, in which HIF-1 $\alpha$  and MMP2 play critical roles [40,42]. Furthermore, p-STAT3 upregulated MMP2 expression, which promoted the formation of VM [42]. In previous experiments, we identified that Cyr61 activates the FAK signaling pathway (Fig. 4C, D). Since FAK activation can stimulate the FAK/MEK/ERK signaling pathway to activate transcription factors [43], we hypothesized that Cyr61 promotes VM formation *via* the  $\alpha_V\beta_5$ /FAK signaling cascade to activate HIF-1 $\alpha$  and MMP2. We then verified this

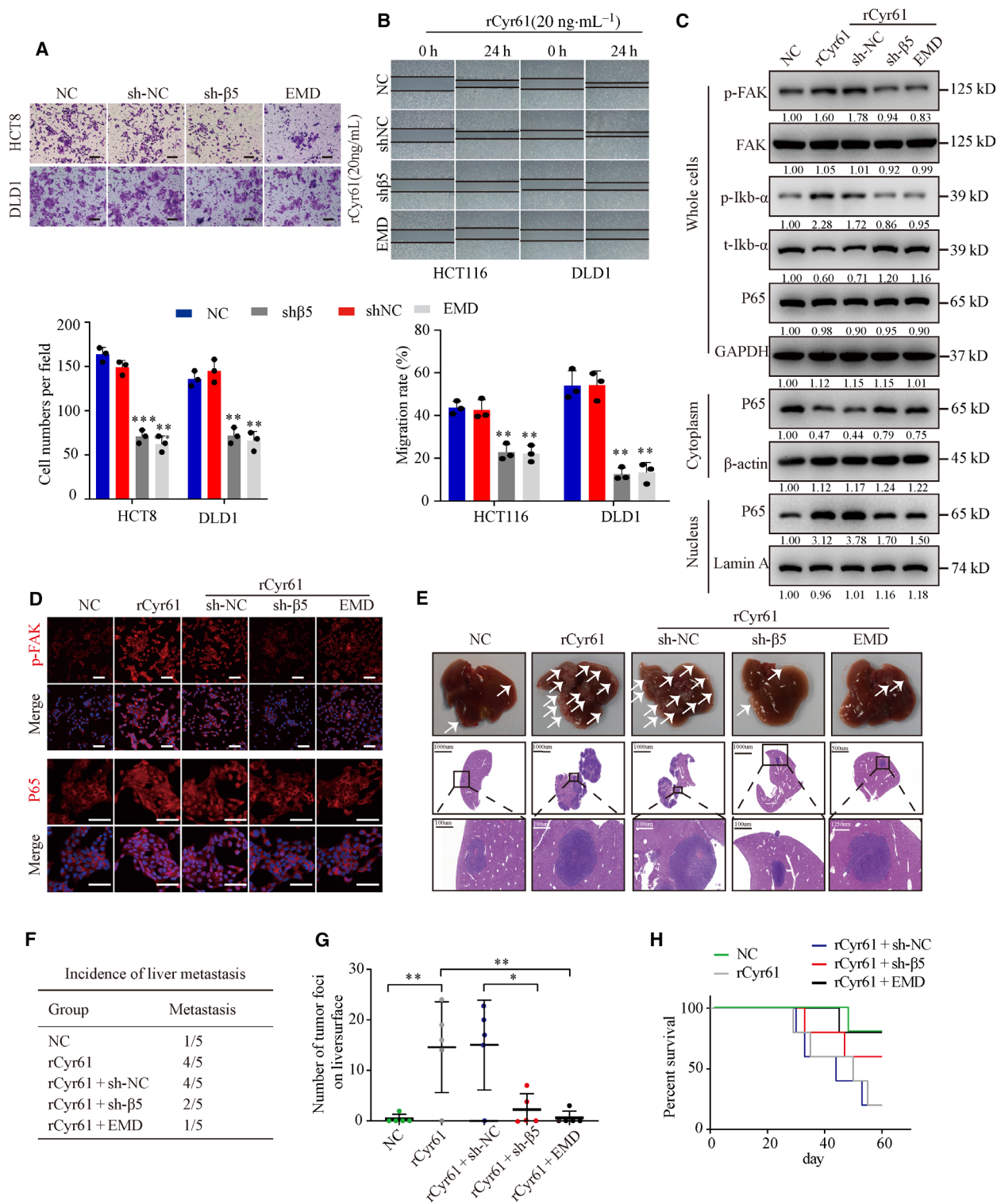
hypothesis in subcutaneous tumors, and the results suggested that these two transcription factors were active after rCyr61 treatment. Consistently, sh $\beta_5$  or EMD treatment suppressed this signaling cascade (Fig. 5F and Fig. S5A). Emerging evidence indicated that VM was related to clinical stage [44] and tumor metastasis [45], with a relationship between VM and the existence of CTCs [46]. Flow cytometric analysis of CTCs in whole-blood samples from the mice showed that treatment with rCyr61 increased the number of CTCs compared to the control group. Conversely, treatment with sh $\beta_5$  or EMD decreased the number of CTCs (Fig. 5G and Fig. S5B).

Next, we applied a 3D culture system to identify VM formation *in vitro*. HCT8 and HCT116 cells treated with rCyr61 showed vessel-like structures, while CRC cells treated with sh $\beta_5$  or EMD spread evenly on the matrix surface in a pattern that was similar to that observed in the control group (Fig. 5H,I). Moreover, western blot analysis was performed to confirm the ability of Cyr61 to activate HIF-1 $\alpha$  and MMP2 *in vitro*. As expected, the protein level of HIF-1 $\alpha$  and MMP2 were increased *via* the FAK/MEK/ERK signaling activation pathway (Fig. 5J and Fig. S5C). We further analyzed the protein levels of integrin  $\alpha_V\beta_5$ /FAK/HIF-1 $\alpha$ /STAT3/MMP2 signaling cascade *via* IF assays. Compared with the controls, IF assays revealed upregulated expression of p-FAK, p-MEK, and MMP2 and intense nuclear staining of ERK, HIF-1 $\alpha$ , and STAT3 in CRC cells treated with rCyr61 (Fig. S5D). Taken together, these results suggested that Cyr61 enhances VM formation to promote CRC growth and metastasis *in vivo* and *in vitro* *via* the integrin  $\alpha_V\beta_5$ /FAK/HIF-1 $\alpha$ /STAT3/MMP2 signaling cascade.

### 3.6. Cyr61 is related to VM formation in CRC tissues

We further investigated VM formation and the expression levels of proteins related to the FAK/HIF-1 $\alpha$ /

**Fig. 4.** Cyr61 promotes CRC cell migration and invasion *via*  $\alpha_V\beta_5$ /FAK/NF- $\kappa$ B signaling pathway. (A) Representative images of transwell migration assays for HCT8 and DLD1 cells with integrin  $\beta_5$  knockdown or treated with integrin  $\alpha_V\beta_5$  inhibitor EMD 121974 (EMD) before treated with rCyr61 (20 ng·mL<sup>−1</sup>). Scale bar = 100  $\mu$ m,  $n = 3$ . (B) Representative images of wound-healing assays for HCT116 and DLD1 cells with integrin  $\beta_5$  knockdown or treated with integrin  $\alpha_V\beta_5$  inhibitor EMD before treated with rCyr61 (20 ng·mL<sup>−1</sup>).  $n = 3$ . (C) Western blot analysis the expression of p-FAK, FAK, p-I $\kappa$ B- $\alpha$ , t-I $\kappa$ B- $\alpha$ P65, and P65 in HCT8 cells with integrin  $\beta_5$  knockdown or with integrin  $\alpha_V\beta_5$  inhibitor EMD. GAPDH,  $\beta$ -actin, and Lamin A were used as the controls. (D) Confocal microscopy assays were performed to detect the expression of p-FAK and subcellular localization of P65 in HCT8 cells with integrin  $\beta_5$  knockdown or treated with integrin  $\alpha_V\beta_5$  inhibitor EMD. Scale bar = 50  $\mu$ m. (E) Autopsy and H&E staining of the livers in the nude mice by *in vivo* liver metastasis assays ( $n = 5$  per group). The arrows indicated the liver metastasis. Black scale bar = 1000  $\mu$ m. White scale bar = 100  $\mu$ m. (F) Incidence of liver metastasis in the nude mice *in vivo* liver metastasis assays. (G) Number of tumor foci on liver surface in the nude mice *in vivo* liver metastasis assays. (H) Kaplan–Meier survival analysis of the nude mice. NC, negative control. Values are represented as mean  $\pm$  SD. \* $P < 0.05$ , \*\* $P < 0.01$ , \*\*\* $P < 0.001$ , by two-tailed Student's  $t$ -test and one-way ANOVA (A, B, G).



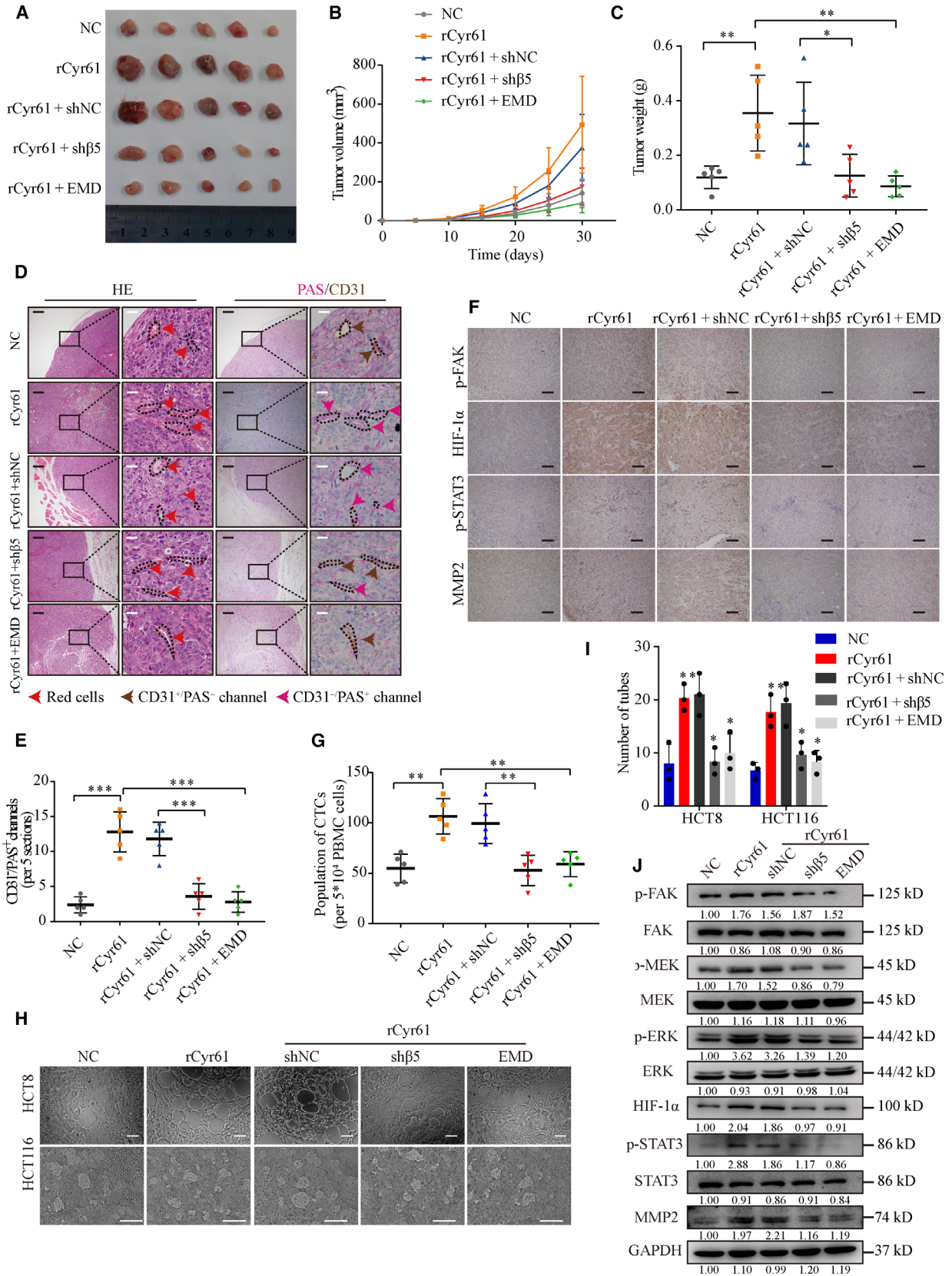


**Fig. 5.** Cyr61 promotes VM formation to promote CRC progression *via* integrin  $\alpha_v\beta_5$ . (A) Tumors in nude mice subcutaneously injected with HCT8 cells pretreated with rCyr61, EMD, or knockdown integrin  $\beta_5$  expression ( $n = 5$  per group). (B) Growth curves of the xenograft tumors. (C) Tumor weight of the HCT8 xenograft tumors. (D) H&E, PAS, and CD31 staining in xenograft tumors. Red arrows indicate the presence of red blood cells; brown arrows indicate typical blood vessels with CD31<sup>+</sup> staining; pink arrows indicate PAS<sup>+</sup>/CD31<sup>-</sup> VM channels. Black scale bars = 200  $\mu\text{m}$ , white scale bars = 20  $\mu\text{m}$ . (E) The numbers of PAS<sup>+</sup>/CD31<sup>-</sup> VM channels in xenograft tumors. (F) IHC analysis of p-FAK, HIF-1 $\alpha$ , p-STAT3, and MMP2 expression in xenograft tumors. Scale bars = 100  $\mu\text{m}$ . (G) Statistics of the flow cytometric analysis of the GFP labeled CTCs from whole blood in the nude mice. (H, I) Representative images and statistics of tube formation in HCT8 and HCT116 cells pretreated with rCyr61, EMD, or knockdown integrin $\beta_5$  expression. Scale bars = 100  $\mu\text{m}$ ,  $n = 3$ . (J) Western blot analysis of  $\alpha_v\beta_5$ /FAK/HIF-1 $\alpha$ /STAT3/MMP2 signaling cascade in HCT8 cells pretreated with rCyr61, EMD, or knockdown integrin  $\beta_5$  expression. NC, negative control. Values are represented as mean  $\pm$  SD. \* $P < 0.05$ , \*\* $P < 0.01$ , \*\*\* $P < 0.001$ , by 2-tailed Student's *t*-test and one-way ANOVA (C, E, G, I).

STAT3/MMP2 signaling cascade in CRC tissues with or without metastasis. Forty cases of CRC tissues, half of which were with metastasis, were selected from 364 CRC patients whose serum Cyr61 protein levels had been analyzed before. Compared with the cases without metastasis, we found that the number of PAS<sup>+</sup>/CD31<sup>-</sup> vascular-like channels increased in CRC tissues with metastasis (Fig. 6A,B). IHC analysis showed that the protein levels of p-FAK, HIF-1 $\alpha$ , p-STAT3, and MMP2 were also upregulated in CRC tissues with metastasis (Fig. 6A). Moreover, the numbers of PAS<sup>+</sup>/CD31<sup>-</sup> vascular-like channels correlated positively with serum Cyr61 protein levels and the levels of p-FAK, HIF-1 $\alpha$ , p-STAT3, and MMP2 protein in tissues (Fig. 6C–G). Thus, these data indicated the existence of VM in CRC tissues and further confirmed the association between VM formation, metastasis, and activation of the FAK/HIF-1 $\alpha$ /STAT3/MMP2 signaling cascade.

### 3.7. Synergistic effect of anti-VM by integrin $\alpha_v\beta_5$ inhibitor EMD and anti-VEGF by bevacizumab therapy in CRC PDX models

Since angiogenesis plays a vital role in CRC growth and metastasis, anti-VEGF therapy is a useful treatment strategy [47]. PDX models retain the characteristics of the original cancer and are used for curative effect analysis and preclinical drug evaluation [48]. Therefore, we analyzed the synergistic effect of integrin  $\alpha_v\beta_5$  inhibitor EMD and bevacizumab, a widely used anti-VEGF monoclonal antibody, in two PDX models. Treatment with EMD or bevacizumab alone inhibited tumor growth moderately compared to the control group. Notably, the combination of EMD and bevacizumab significantly inhibited tumor growth (Fig. 7A, B). Next, we analyzed the number of VM channels and microvessels in PDX tumors by double staining of PAS and CD31. Treatment with bevacizumab decreased the number of CD31<sup>+</sup> microvessels. Furthermore, EMD treatment significantly decreased the number of PAS<sup>+</sup>/

CD31<sup>-</sup> channels and moderately decreased the number of CD31<sup>+</sup> microvessels. Combination treatment with EMD and bevacizumab markedly decreased both channel formation (Fig. 7C–F). Taken together, these data suggested that combination of anti-VM by EMD and anti-VEGF by bevacizumab was a novel therapeutic strategy for CRC.

### 3.8. CRC cell-derived exosomal STAT3 promotes Cyr61 transcription

We finally investigated the potential mechanisms underlying the increased secretion of Cyr61 in ADSCs isolated from CRC patients. It had been reported that Cyr61 is a target gene of STAT3 in embryonic stem cells [49]. Therefore, we speculated that STAT3 plays a vital role in Cyr61 transcription in ADSCs. Western blot analysis showed that the protein levels of STAT3 and p-STAT3 were increased in ADSCs-CRC compared to ADSCs-NC (Fig. 8A). More importantly, STAT3 inhibitors suppressed Cyr61 RNA levels significantly (Fig. 8B). Next, we cloned a fragment containing the Cyr61 promoter into a luciferase reporter vector and the results indicated that STAT3 markedly increased the luciferase activity (Fig. 8C). The potential STAT3-binding site (–1414 to –1404 bp) was predicted by the JASPAR database. To identify the binding site, a series of reporter vectors containing sequential deletions of the Cyr61 promoter were transfected into ADSCs. As shown in Fig. 8D, the –1414 to –1404 bp region was identified as the potential STAT3-binding site. Mutation of four nucleotides at the STAT3-binding site decreased the luciferase activity (Fig. 8E). CHIP assays were performed to further verify the direct interaction between STAT3 and the –1414 to –1404 bp region (Fig. 8F,G). Altogether, these data suggested that STAT3 is involved in Cyr61 transcription.

Next, we investigated the mechanism by which STAT3 and p-STAT3 are upregulated in ADSCs-CRC and the potential influence of tumor cells. Cocultured

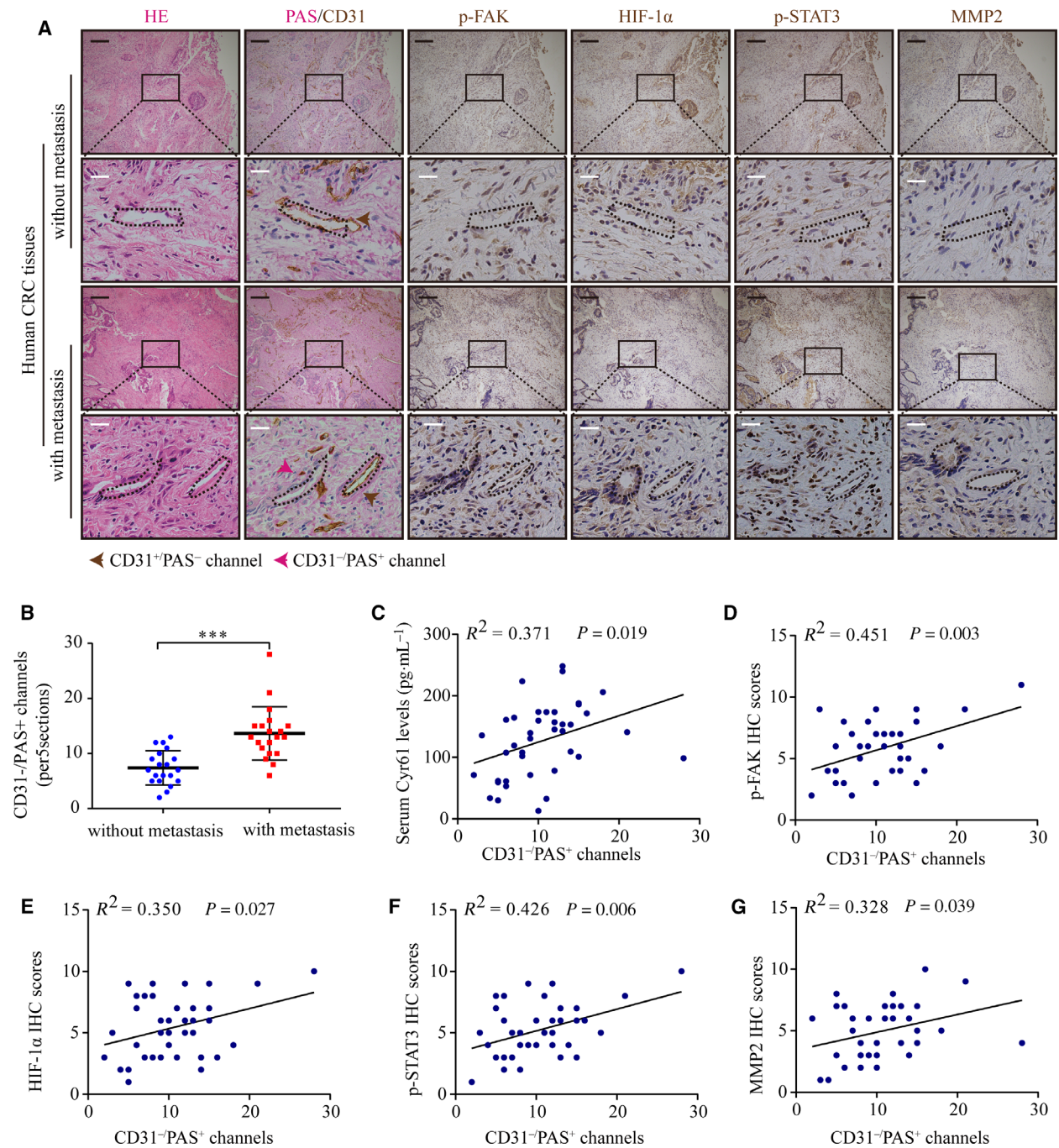


**Fig. 6.** The relationship between serum Cyr61 levels and VM in CRC tissues. (A) H&E staining, VM formation, p-FAK, HIF-1 $\alpha$ , p-STAT3, and MMP2 expression in CRC patients with or without metastasis.  $n = 20$  per group. Black scale bars = 200  $\mu$ m; white scale bars = 20  $\mu$ m. (B) Statistics of PAS<sup>+</sup>/CD31<sup>-</sup> VM channels in CRC patients with or without metastasis. (C–G) Pearson correlation of PAS<sup>+</sup>/CD31<sup>-</sup> VM channels with serum Cyr61 levels, p-FAK, HIF-1 $\alpha$ , p-STAT3, and MMP2 IHC scores in CRC tissues. Values are represented as mean  $\pm$  SD. \*\*\* $P < 0.001$ , by two-tailed Student's  $t$ -test (B).

of ADSCs with CRC cells resulted in increased protein levels of STAT3 and p-STAT3 (Fig. 8H) and increased Cyr61 RNA levels (Fig. 8I). Accumulating evidence suggests that exosomes play a vital role in cell-to-cell

communication through transfer of exosomal contents [50]. We identified the existence of STAT3 and p-STAT3 proteins in exosomes extracted from the culture medium of normal colonic cell and three CRC cell

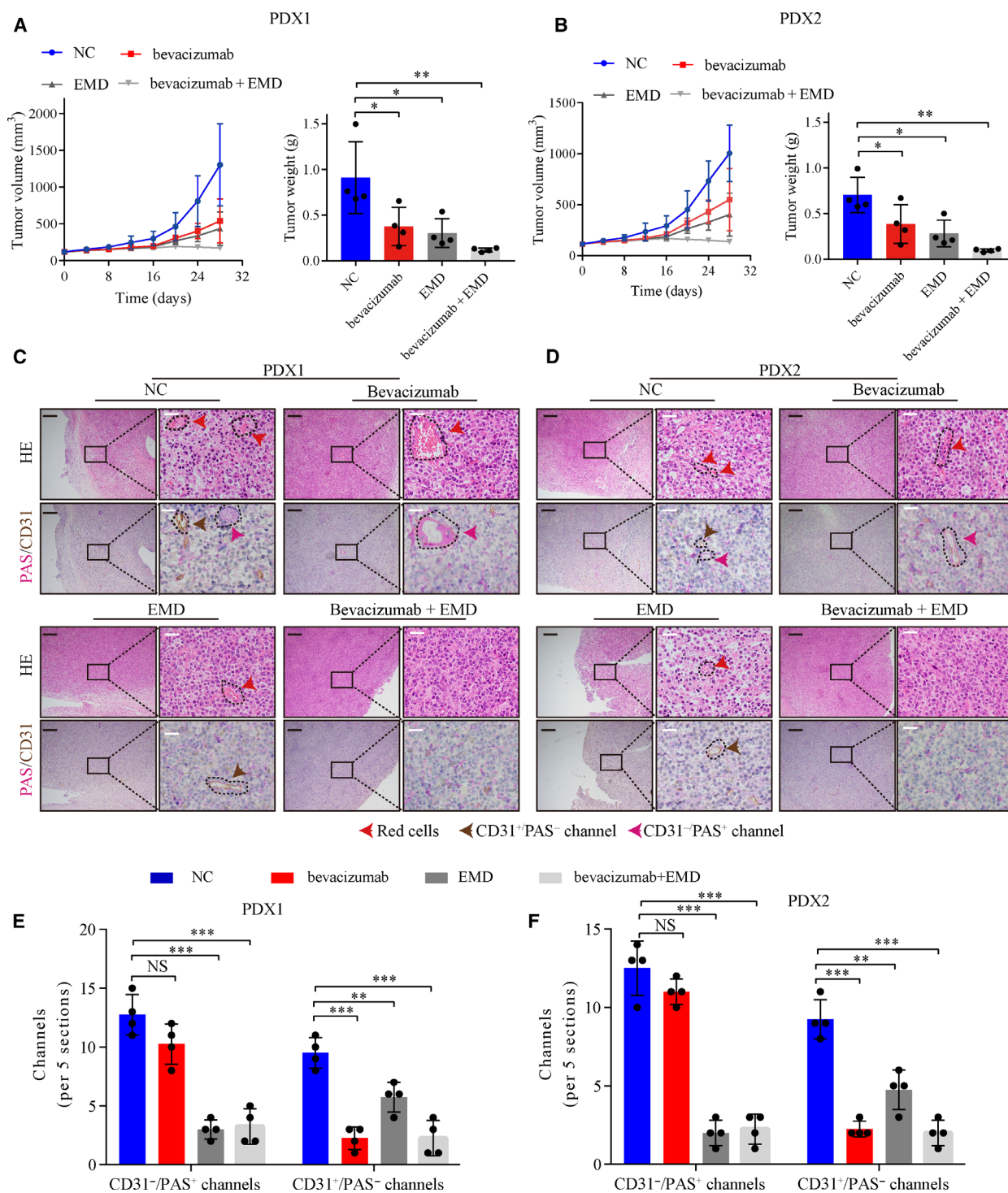
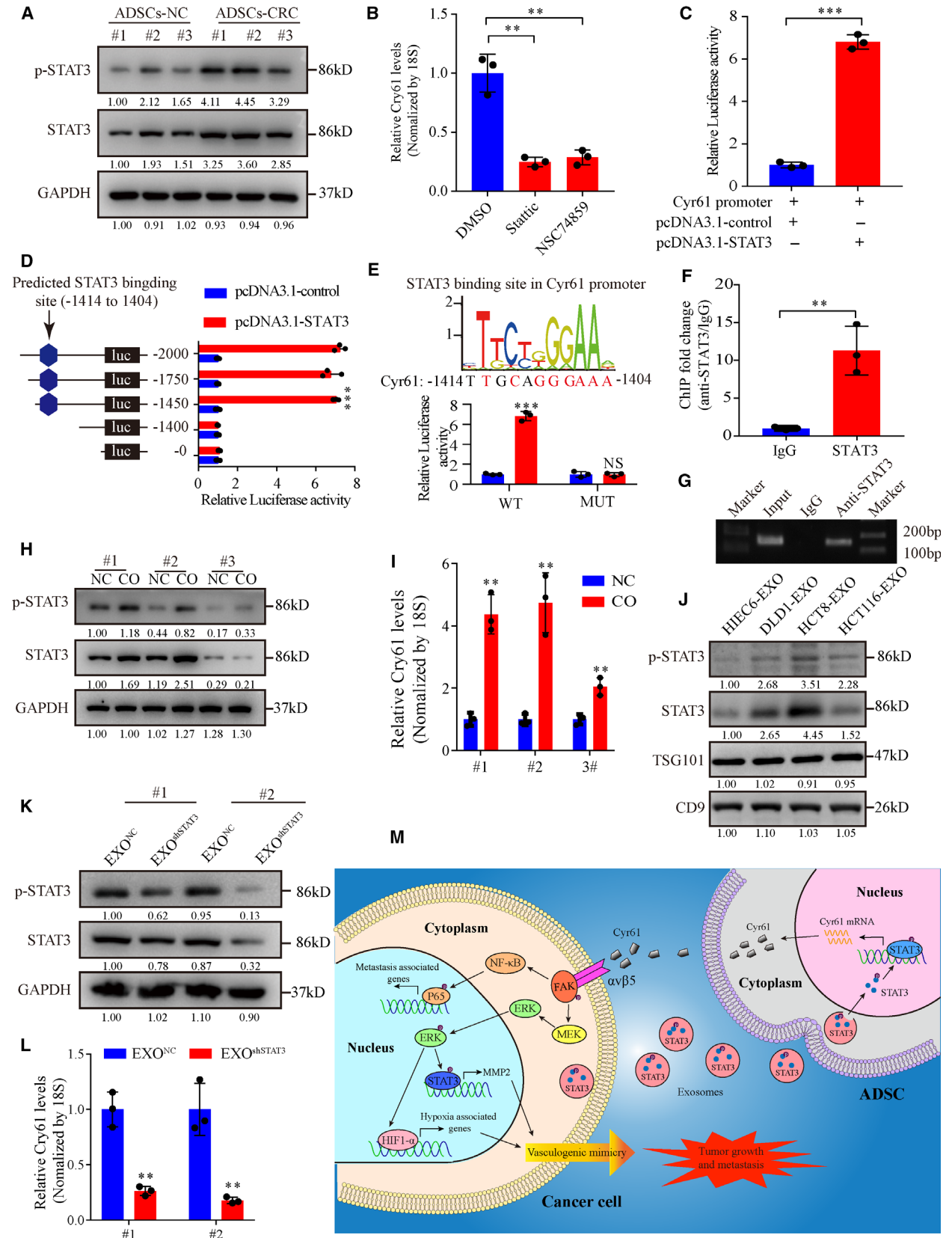


**Fig. 7.** Synergistic effect of EMD and bevacizumab in CRC PDX models. (A, B) Growth curves and tumor weight of PDX model tumors after treatment with vehicle, EMD, or/and bevacizumab. (*n* = 4) (C, D) H&E, PAS, and CD31 staining in PDX model tumors after treatment with vehicle, EMD, or/and bevacizumab. Black scale bars = 200 μm; white scale bars = 20 μm, *n* = 4. (E, F) Statistics of PAS<sup>+</sup>/CD31<sup>-</sup> VM channels and PAS<sup>-</sup>/CD31<sup>+</sup> channels in PDX model tumors after treatment with vehicle, EMD or/and bevacizumab. Values are represented as mean ± SD. NC, negative control. NS, no significant, \**P* < 0.05, \*\**P* < 0.01, \*\*\**P* < 0.001, by one-way ANOVA (A, B, E, F).



lines (Fig. 8J). Furthermore, exosomal STAT3 and p-STAT3 levels in STAT3 knockdown HCT8 cells were consistent with those changes in the parental cells (Fig. S6A,B). To further identify the function of tumor-derived exosomal STAT3 and p-STAT3 in ADSCs, we cocultured ADSCs with these exosomes. We found the protein levels of STAT3 and p-STAT3 and the RNA levels of Cyr61 were decreased when ADSCs were cocultured with EXO<sup>shSTAT3</sup> (Fig. 8K,L). These findings suggested that CRC cell-derived exosomal STAT3 and p-STAT3 play a vital role in Cyr61 transcription.

#### 4. Discussion

Cyr61, also known as CCN1, has diverse biological functions, such as promoting cell migration and proliferation by binding to cell-specific integrin receptors [22]. A previous study also showed that Cyr61 was upregulated in the serum of CRC patients [21]. However, the source of serum Cyr61 and the mechanisms by which Cyr61 promotes CRC progression still remain unknown. In this study, we found that CRC-associated ADSCs secreted more Cyr61 than ADSCs-NC and the serum Cyr61 levels were associated with advanced TNM stages. Mechanistically, Cyr61 promoted CRC cell metastasis *in vitro* and *in vivo* by activating integrin  $\alpha_V\beta_5$ . In addition, Cyr61 could promote VM formation to promote CRC progression *via* integrin  $\alpha_V\beta_5$ . Moreover, a synergistic effect of anti-VM by integrin  $\alpha_V\beta_5$  inhibitor and anti-VEGF by bevacizumab therapy was identified in PDX models. These findings indicated that Cyr61 derived from ADSCs plays a critical role in promoting CRC progression *via* integrin  $\alpha_V\beta_5$  and provided a novel antitumor strategy.

Instead of canonical RGD sequence, Cyr61 contained the noncanonical RGD sequence that mediates binding to various integrins [51]. The interaction of

Cyr61 with different integrin receptors contributes to their specific functions. Cyr61 interacts with integrin  $\alpha_V\beta_3$ ,  $\alpha_V\beta_5$ , and  $\alpha_6\beta_1$  to stimulate fibroblasts cell DNA synthesis, adhesion, and migration, respectively [52]. Cyr61 stimulates endothelial cell and vascular smooth muscle cell migration by binding to  $\alpha_V\beta_3$  and  $\alpha_6\beta_1$  [23]. Mutational analysis indicated that Cyr61 function by binding to specific integrin receptors independently of one another [53]. In this study, we demonstrated that serum Cyr61 was derived mainly from ADSCs rather than the tumor itself. Serum Cyr61 exhibited a better diagnostic value (AUC = 0.933) for CRC compared to CEA and CA199, suggesting that serum Cyr61 exhibits higher sensitivity and specificity as a diagnostic marker. Thus, we propose that plasma Cyr61 is a new promising new biomarker for the diagnosis and prognosis of CRC. Moreover, we identified integrin  $\alpha_V\beta_5$  as the functional receptor of Cyr61 on CRC cells and showed that Cyr61 interacted directly with integrin  $\alpha_V\beta_5$  to activate the downstream FAK signaling pathway to promote CRC progression.

Vasculogenic mimicry, a vascular channel-like structure that consists of tumor cells but not ECs, was first reported in in uveal melanoma in 1999 [54]. VM formation is identified by positive PAS staining in the absence of CD31 expression and red blood cells in the vascular-like channels [41]. VM has been identified in various malignant tumors, including CRC [55]. Hypoxic tumor microenvironment was a common phenomenon because of vast oxygen consuming [56]. Tumor microenvironment becomes hypoxic increasingly with tumor growth. Under hypoxic condition, cancer cells undergo adaptive changes, such as HIF-1 $\alpha$  activation. HIF-1 $\alpha$  and MMP2 play critical roles in VM formation [40,42]. Previous studies demonstrated that STAT3 blocks HIF-1 $\alpha$  degradation and accelerates its de novo synthesis to enhance its stability and activity [42]. In addition, p-STAT3 upregulates MMP2 expression to promote the formation of VM [42]. In

**Fig. 8.** CRC cell-derived exosomal STAT3 promotes Cyr61 transcription. (A) Western blot analysis of p-STAT3 and STAT3 expression in ADSCs-NC and ADSCs-CRC. (B) qRT-PCR analysis of Cyr61 mRNA levels in ADSCs treated with STAT3 inhibitors.  $n = 3$ . (C) Luciferase activity of the Cyr61 promoter in ADSCs transfected with STAT3.  $n = 3$ . (D) Luciferase (luc) reporter assays for ADSCs transfected with a series of reporter vectors containing sequential deletion of the Cyr61 promoter.  $n = 3$ . (E) Potential STAT3-binding site in the Cyr61 promoter predicted in the JASPAR database. Luciferase reporter assays for ADSCs transfected with reporter plasmids containing point mutation at the STAT3-binding site.  $n = 3$ . (F, G) qRT-PCR analysis of the product of chromatin immunoprecipitation assays for the binding of STAT3 to the crucial STAT3-binding site in the Cyr61 promoter. (H) Western blot analysis of p-STAT3 and STAT3 expression changes in ADSCs cocultured with HCT8 cells. (I) qRT-PCR analysis of Cyr61 mRNA levels in ADSCs cocultured with HCT8 cells.  $n = 3$ . (J) Western blot analysis of p-STAT3 and STAT3 in normal colonic cell and CRC cell-derived exosomes. (K) Western blot analysis of p-STAT3 and STAT3 expression in ADSCs cocultured with CRC cell-derived exosomes with or without p-STAT3 and STAT3 knockdown. (L) qRT-PCR analysis of Cyr61 mRNA levels in ADSCs cocultured with CRC cell-derived exosomes with or without p-STAT3 and STAT3 knockdown.  $n = 3$ . (M) Schematic model of the role of Cyr61 in CRC tumor progression. Values are represented as mean  $\pm$  SD. CO, cocultured; EXO, exosomes. NS, no significant, \*\* $P < 0.01$ , \*\*\* $P < 0.001$ , by two-tailed Student's *t*-test (C, E, F, I, L) and one-way ANOVA (B, D).

this study, the *in vitro* experiments indicated that CRC cell proliferation was not influenced by Cyr61, which seemed to be inconsistent with the subcutaneous xenografts assays which showed that Cyr61 increased the volume and weight of tumors (Fig. 5A–C). This can be explained by the findings that Cyr61 binds to its functional receptor integrin  $\alpha_v\beta_5$  to activate FAK signaling pathway, thereby upregulating the expression of HIF-1 $\alpha$  and MMP2, and ultimately stimulating VM formation to promote CRC cell proliferation *in vivo*.

Anti-angiogenesis is a promising treatment in CRC. Bevacizumab, a widely used anti-VEGF monoclonal antibody, has been evaluated in a multicenter phase II clinical trial in CRC patients with metastasis [57]. However, anti-angiogenesis with VEGF inhibitors causes a hypoxic tumor microenvironment that may promote tumor progression through VM formation. Therefore, anti-VM therapy combined with anti-VEGF to block the supply of oxygen and nutrition to cancer cells is a strategy to overcome the side effect of anti-VEGF therapy. In this study, we found that Cyr61 promoted VM formation by binding to integrin  $\alpha_v\beta_5$ . The integrin  $\alpha_v\beta_5$  inhibitor cilengitide (EMD) has been evaluated in clinical trials in non-small-cell lung cancer and glioblastoma [58,59]. Combination treatment with EMD and bevacizumab decreased the number of VM channels and microvessels in CRC PDX models. This indicated the potential of cilengitide for clinical application in CRC treatment. In addition to integrin  $\alpha_v\beta_5$ , targeting serum Cyr61 or the integrin  $\alpha_v\beta_5$ /FAK signaling pathway may also decrease tumor progression.

## 5. Conclusions

Our findings revealed that ADSC-derived Cyr61 promotes CRC metastasis and VM formation *via* its functional receptor integrin  $\alpha_v\beta_5$  to activate the FAK signaling pathway (Fig. 8M). Moreover, combination therapy with cilengitide and bevacizumab is implicated as a potential novel antitumor strategy for CRC.

## Acknowledgements

This work was supported by National Key R&D Program of China (2017YFC1308800), National Natural Science Foundation of China (81870383), Clinical Innovation Research Program of Bioland Laboratory (Guangzhou Regenerative Medicine and Health Guangdong Laboratory) (No. 2018GZR0201005), and Science and Technology Planning Project of Guangzhou City (201804010014).

## Conflict of interest

All authors declare no conflict of interests.

## Data accessibility

The mass spectrometry data have been deposited to the ProteomeXchange Consortium *via* the PRIDE [60] partner repository with the dataset identifier PXD019954.

## Author contributions

ZL performed *in vitro* experiments; ZL and HL performed animal study together; YZ and XW performed the ISH scoring analyses; YZ, ZZ, FW, and XH helped to organize and analyze the data; ZL drafted this manuscript and PL and XW corrected it; PL and XW supervised this study and provided funding.

## Peer Review

The peer review history for this article is available at <https://publons.com/publon/10.1002/1878-0261.12998>.

## References

- 1 Bray F, Ferlay J, Soerjomataram I, Siegel RL, Torre LA & Jemal A (2018) Global cancer statistics 2018: GLOBOCAN estimates of incidence and mortality worldwide for 36 cancers in 185 countries. *CA Cancer J Clin* **68**, 394–424.
- 2 Fidler IJ (2003) The pathogenesis of cancer metastasis: the 'seed and soil' hypothesis revisited. *Nat Rev Cancer* **3**, 453–458.
- 3 Christofori G (2006) New signals from the invasive front. *Nature* **441**, 444–450.
- 4 McGown C, Biredinc A & Younossi ZM (2014) Adipose tissue as an endocrine organ. *Clin Liver Dis* **18**, 41–58.
- 5 Calle EE, Rodriguez C, Walker-Thurmond K & Thun MJ (2003) Overweight, obesity, and mortality from cancer in a prospectively studied cohort of U.S. adults. *N Engl J Med* **348**, 1625–1638.
- 6 Terry PD, Miller AB & Rohan TE (2002) Obesity and colorectal cancer risk in women. *Gut* **51**, 191–194.
- 7 Lee YH & Mottillo EP (1842) Granneman JG (2014) Adipose tissue plasticity from WAT to BAT and in between. *Biochim Biophys Acta* **3**, 358–369.
- 8 Razmkhah M, Jaberipour M, Erfani N, Habibagahi M, Talei AR & Ghaderi A (2011) Adipose derived stem cells (ASCs) isolated from breast cancer tissue express IL-4, IL-10 and TGF-beta1 and upregulate expression of regulatory molecules on T cells: do they protect

- breast cancer cells from the immune response? *Cell Immunol* **266**, 116–122.
- 9 Chandler EM, Seo BR, Califano JP, Andresen Eguiluz RC, Lee JS, Yoon CJ, Tims DT, Wang JX, Cheng L, Mohanan S *et al.* (2012) Implanted adipose progenitor cells as physicochemical regulators of breast cancer. *Proc Natl Acad Sci USA* **109**, 9786–9791.
  - 10 Klopp AH, Zhang Y, Solley T, Amaya-Manzanares F, Marini F, Andreeff M, Debeb B, Woodward W, Schmandt R, Broaddus R *et al.* (2012) Omental adipose tissue-derived stromal cells promote vascularization and growth of endometrial tumors. *Clin Cancer Res* **18**, 771–782.
  - 11 Heo SC, Lee KO, Shin SH, Kwon YW, Kim YM, Lee CH, Kim YD, Lee MK, Yoon MS & Kim JH (2011) Periostin mediates human adipose tissue-derived mesenchymal stem cell-stimulated tumor growth in a xenograft lung adenocarcinoma model. *Biochim Biophys Acta* **1813**, 2061–2070.
  - 12 Chu Y, Wang Y, Peng W, Xu L, Liu M, Li J, Hu X, Li Y, Zuo J & Ye Y (2018) STAT3 activation by IL-6 from adipose-derived stem cells promotes endometrial carcinoma proliferation and metastasis. *Biochem Biophys Res Commun* **500**, 626–631.
  - 13 Visweswaran M, Keane KN, Arfuso F, Dilley RJ, Newsholme P & Dharmarajan A (2018) The influence of breast tumour-derived factors and Wnt antagonism on the transformation of adipose-derived mesenchymal stem cells into tumour-associated fibroblasts. *Cancer Microenviron* **11**, 71–84.
  - 14 Cho JA, Park H, Lim EH & Lee KW (2012) Exosomes from breast cancer cells can convert adipose tissue-derived mesenchymal stem cells into myofibroblast-like cells. *Int J Oncol* **40**, 130–138.
  - 15 Kim WS, Park SH, Ahn SJ, Kim HK, Park JS, Lee GY, Kim KJ, Whang KK, Kang SH, Park BS *et al.* (2008) Whitening effect of adipose-derived stem cells: a critical role of TGF- $\beta$  1. *Biol Pharm Bull* **31**, 606–610.
  - 16 Ning H, Lin G, Fandel T, Banie L, Lue TF & Lin CS (2008) Insulin growth factor signaling mediates neuron-like differentiation of adipose-tissue-derived stem cells. *Differentiation* **76**, 488–494.
  - 17 Song YH, Gehmert S, Sadat S, Pinkernell K, Bai X, Matthias N & Alt E (2007) VEGF is critical for spontaneous differentiation of stem cells into cardiomyocytes. *Biochem Biophys Res Commun* **354**, 999–1003.
  - 18 O'Kelly J, Chung A, Lemp N, Chumakova K, Yin D, Wang HJ, Said J, Gui D, Miller CW, Karlan BY *et al.* (2008) Functional domains of CCN1 (Cyr61) regulate breast cancer progression. *Int J Oncol* **33**, 59–67.
  - 19 Zhao ZS, Li L, Wang HJ & Wang YY (2011) Expression and prognostic significance of CEACAM6, ITGB1, and CYR61 in peripheral blood of patients with gastric cancer. *J Surg Oncol* **104**, 525–529.
  - 20 Feng P, Wang B & Ren EC (2008) Cyr61/CCN1 is a tumor suppressor in human hepatocellular carcinoma and involved in DNA damage response. *Int J Biochem Cell Biol* **40**, 98–109.
  - 21 Song YF, Xu ZB, Zhu XJ, Tao X, Liu JL, Gao FL, Wu CL, Song B & Lin Q (2017) Serum Cyr61 as a potential biomarker for diagnosis of colorectal cancer. *Clin Transl Oncol* **19**, 519–524.
  - 22 Lau LF (2011) CCN1/CYR61 the very model of a modern matricellular protein. *Cell Mol Life Sci* **68**, 3149–3163.
  - 23 Leu SJ, Lam SC & Lau LF (2002) Pro-angiogenic activities of CYR61 (CCN1) mediated through integrins  $\alpha$ 3 $\beta$ 1 and  $\alpha$ 6 $\beta$ 1 in human umbilical vein endothelial cells. *J Biol Chem* **277**, 46248–46255.
  - 24 Lin MT, Zuon CY, Chang CC, Chen ST, Chen CP, Lin BR, Wang MY, Jeng YM, Chang KJ, Lee PH *et al.* (2005) Cyr61 induces gastric cancer cell motility/invasion via activation of the integrin/nuclear factor- $\kappa$ B/cyclooxygenase-2 signaling pathway. *Clin Cancer Res* **11**, 5809–5820.
  - 25 Xie L, Song X, Lin H, Chen Z, Li Q, Guo T, Xu T, Su T, Xu M, Chang X *et al.* (2019) Aberrant activation of CYR61 enhancers in colorectal cancer development. *J Exp Clin Cancer Res* **38**, 213.
  - 26 Han S, Bui NT, Ho MT, Kim YM, Cho M & Shin DB (2016) Dexamethasone inhibits TGF- $\beta$ 1-induced cell migration by regulating the ERK and AKT pathways in human colon cancer cells via CYR61. *Cancer Res Treat* **48**, 1141–1153.
  - 27 Monnier Y, Farmer P, Bieler G, Imaizumi N, Sengstag T, Alghisi GC, Stehle JC, Ciarloni L, Andrejevic-Blant S, Moeckli R *et al.* (2008) CYR61 and  $\alpha$ 5 $\beta$ 1 integrin cooperate to promote invasion and metastasis of tumors growing in preirradiated stroma. *Cancer Res* **68**, 7323–7331.
  - 28 Estrada R, Li N, Sarojini H, An J, Lee MJ & Wang E (2009) Secretome from mesenchymal stem cells induces angiogenesis via Cyr61. *J Cell Physiol* **219**, 563–571.
  - 29 Ghasemi N, Razavi S, Mardani M, Esfandiari E, Salehi H & Zarkesh Esfahani SH (2014) Transplantation of human adipose-derived stem cells enhances remyelination in lysoclethrin-induced focal demyelination of rat spinal cord. *Mol Biotechnol* **56**, 470–478.
  - 30 Liang ZX, Liu HS, Wang FW, Xiong L, Zhou C, Hu T, He XW, Wu XJ, Xie D, Wu XR *et al.* (2019) LncRNA RPPH1 promotes colorectal cancer metastasis by interacting with TUBB3 and by promoting exosomes-mediated macrophage M2 polarization. *Cell Death Dis* **10**, 829.
  - 31 Ohara Y, Oda T, Sugano M, Hashimoto S, Enomoto T, Yamada K, Akashi Y, Miyamoto R, Kobayashi A, Fukunaga K *et al.* (2013) Histological and prognostic importance of CD44(+) /CD24(+) /EpCAM(+)

- expression in clinical pancreatic cancer. *Cancer Sci* **104**, 1127–1134.
- 32 Yuan JH, Yang F, Chen BF, Lu Z, Huo XS, Zhou WP, Wang F & Sun SH (2011) The histone deacetylase 4/SP1/microrna-200a regulatory network contributes to aberrant histone acetylation in hepatocellular carcinoma. *Hepatology* **54**, 2025–2035.
- 33 Yuan JH, Yang F, Wang F, Ma JZ, Guo YJ, Tao QF, Liu F, Pan W, Wang TT, Zhou CC *et al.* (2014) A long noncoding RNA activated by TGF-beta promotes the invasion-metastasis cascade in hepatocellular carcinoma. *Cancer Cell* **25**, 666–681.
- 34 Brigstock DR (2003) The CCN family a new stimulus package. *J Endocrinol* **178**, 169–175.
- 35 Brigstock DR (1999) The connective tissue growth factor/cysteine-rich 61/nephroblastoma overexpressed (CCN) family. *Endocr Rev* **20**, 189–206.
- 36 Holbourn KP, Acharya KR & Perbal B (2008) The CCN family of proteins: structure-function relationships. *Trends Biochem Sci* **33**, 461–473.
- 37 Karin M (2006) Nuclear factor-kappaB in cancer development and progression. *Nature* **441**, 431–436.
- 38 Chaturvedi MM, Sung B, Yadav VR, Kannappan R & Aggarwal BB (2011) NF-kappaB addiction and its role in cancer: 'one size does not fit all'. *Oncogene* **30**, 1615–1630.
- 39 Dwyer SF, Gao L & Gelman IH (2015) Identification of novel focal adhesion kinase substrates role for FAK in NFkappaB signaling. *Int J Biol Sci* **11**, 404–410.
- 40 Xiang T, Lin YX, Ma W, Zhang HJ, Chen KM, He GP, Zhang X, Xu M, Feng QS, Chen MY *et al.* (2018) Vasculogenic mimicry formation in EBV-associated epithelial malignancies. *Nat Commun* **9**, 5009.
- 41 Hendrix MJ, Sefter EA, Hess AR & Sefter RE (2003) Vasculogenic mimicry and tumour-cell plasticity: lessons from melanoma. *Nat Rev Cancer* **3**, 411–421.
- 42 Xu Q, Briggs J, Park S, Niu G, Kortylewski M, Zhang S, Gritsko T, Turkson J, Kay H, Semenza GL *et al.* (2005) Targeting Stat3 blocks both HIF-1 and VEGF expression induced by multiple oncogenic growth signaling pathways. *Oncogene* **24**, 5552–5560.
- 43 Francescone R, Scully S, Bentley B, Yan W, Taylor SL, Oh D, Moral L & Shao R (2012) Glioblastoma-derived tumor cells induce vasculogenic mimicry through Flk-1 protein activation. *J Biol Chem* **287**, 24821–24831.
- 44 Liu T, Sun B, Zhao X, Gu Q, Dong X, Yao Z, Zhao N, Chi J, Liu N, Sun R *et al.* (2013) HER2/neu expression correlates with vasculogenic mimicry in invasive breast carcinoma. *J Cell Mol Med* **17**, 116–122.
- 45 Wagenblast E, Soto M, Gutierrez-Angel S, Hartl CA, Gable AL, Maceli AR, Erard N, Williams AM, Kim SY, Dickopf S *et al.* (2015) A model of breast cancer heterogeneity reveals vascular mimicry as a driver of metastasis. *Nature* **520**, 358–362.
- 46 Williamson SC, Metcalf RL, Trapani F, Mohan S, Antonello J, Abbott B, Leong HS, Chester CP, Simms N, Polanski R *et al.* (2016) Vasculogenic mimicry in small cell lung cancer. *Nat Commun* **7**, 13322.
- 47 Sun W (2012) Angiogenesis in metastatic colorectal cancer and the benefits of targeted therapy. *J Hematol Oncol* **5**, 63.
- 48 Kopetz S, Lemos R & Powis G (2012) The promise of patient-derived xenografts: the best laid plans of mice and men. *Clin Cancer Res* **18**, 5160–5162.
- 49 Bourillot PY, Aksoy I, Schreiber V, Wianny F, Schulz H, Hummel O, Hubner N & Savatier P (2009) Novel STAT3 target genes exert distinct roles in the inhibition of mesoderm and endoderm differentiation in cooperation with Nanog. *Stem Cells* **27**, 1760–1771.
- 50 Lugea A & Waldron RT (2017) Exosome-mediated intercellular communication between stellate cells and cancer cells in pancreatic ductal adenocarcinoma. *Pancreas* **46**, 1–4.
- 51 Hynes RO (2002) Integrins: bidirectional, allosteric signaling machines. *Cell* **110**, 673–687.
- 52 Chen CC & Lau LF (2009) Functions and mechanisms of action of CCN matricellular proteins. *Int J Biochem Cell Biol* **41**, 771–783.
- 53 Leu SJ, Chen N, Chen CC, Todorovic V, Bai T, Juric V, Liu Y, Yan G, Lam SC & Lau LF (2004) Targeted mutagenesis of the angiogenic protein CCN1 (CYR61). Selective inactivation of integrin alpha6beta1-heparan sulfate proteoglycan coreceptor-mediated cellular functions. *J Biol Chem* **279**, 44177–44187.
- 54 Maniotis AJ, Folberg R, Hess A, Sefter EA, Gardner LM, Pe'er J, Trent JM, Meltzer PS & Hendrix MJ (1999) Vascular channel formation by human melanoma cells *in vivo* and *in vitro*: vasculogenic mimicry. *Am J Pathol* **155**, 739–752.
- 55 Baeten CI, Hillen F, Pauwels P, de Bruine AP & Baeten CG (2009) Prognostic role of vasculogenic mimicry in colorectal cancer. *Dis Colon Rectum* **52**, 2028–2035.
- 56 Zhu P, Ning Y, Yao L, Chen M & Xu C (2010) The proliferation, apoptosis, invasion of endothelial-like epithelial ovarian cancer cells induced by hypoxia. *J Exp Clin Cancer Res* **29**, 124.
- 57 Suzuki N, Hazama S, Nagasaka T, Tanioka H, Iwamoto Y, Negoro Y, Yamauchi M, Kobayashi M, Okuda H, Fujishima N *et al.* (2019) Multicenter phase II study of biweekly CAPIRI plus bevacizumab as second-line therapy in patients with metastatic colorectal cancer (JSWOG-C3 study). *Int J Clin Oncol* **24**, 1223–1230.
- 58 Massabeau C, Khalifa J, Filleron T, Modesto A, Bigay-Game L, Plat G, Dierickx L, Aziza R, Rouquette I, Gomez-Roca C *et al.* (2018) Continuous infusion of cilengitide plus chemoradiotherapy for patients with stage III non-small-cell lung cancer: a phase I study. *Clin Lung Cancer* **19**, e277–e285.

- 59 Khasraw M, Lee A, McCowatt S, Kerestes Z, Buyse ME, Back M, Kichenadasse G, Ackland S & Wheeler H (2016) Cilengitide with metronomic temozolomide, procarbazine, and standard radiotherapy in patients with glioblastoma and unmethylated MGMT gene promoter in ExCentric, an open-label phase II trial. *J Neurooncol* **128**, 163–171.
- 60 Perez-Riverol Y, Csordas A, Bai J, Bernal-Llinares M, Hewapathirana S, Kundu DJ, Inuganti A, Griss J, Mayer G, Eisenacher M *et al.* (2019) The PRIDE database and related tools and resources in 2019: improving support for quantification data. *Nucleic Acids Res* **47** (D1), D442–D450.

## Supporting information

Additional supporting information may be found online in the Supporting Information section at the end of the article.

**Fig. S1.** Characterization of ADSCs.

**Fig. S2.** ADSCs derived Cyr61 have no effect on CRC cell proliferation *in vitro*.

**Fig. S3.** Cyr61 receptor identification on CRC cells.

**Fig. S4.** The  $\alpha_v\beta_5$ /FAK/NF- $\kappa$ B signaling pathway changes in DLD1 cells.

**Fig. S5.** The  $\alpha_v\beta_5$ /FAK/HIF-1 $\alpha$ /STAT3/MMP2 signaling cascade changes after Cyr61 treatment.

**Fig. S6.** Western blot analysis of the efficiency of shRNA for STAT3.

**Table S1.** Correlation between Cyr61 levels and clinicopathologic characteristics of CRC patients.

**Table S2.** The ROC curve assay of CEA, CA199, CA125 and Cyr61.

**Table S3.** List of surface membrane proteins of mass spectrometry results (score>35).

**Table S4.** Oligonucleotide sequences.